SEISMICITY ALONG THE HAWAIIAN ISLANDS RECORDED BY THE PLUME LAND AND OCEAN BOTTOM SEISMOMETER NETWORK

A THESIS SUBMITTED TO THE GRADUATE DIVISION OF THE
UNIVERSITY OF HAWAI‘I IN PARTIAL FULFILLMENT
OF THE REQUIREMENTS FOR THE DEGREE OF

MASTER OF SCIENCE

IN

GEOLOGY AND GEOPHYSICS

DECEMBER 2009

By
Maria C. Anchieta

Thesis Committee:

Cecily J. Wolfe, Chairperson
Frederick Duennebier
Robert Dunn

We certify that we have read this thesis and that, in our opinion, it is satisfactory in scope and quality as a thesis for the degree of Master of Science in Geology and Geophysics.

THESIS COMMITTEE

_____

Chairperson

_____

_____

To good fortune,
the intersection of opportunity,
preparation, and effort.

ACKNOWLEDGEMENTS

First and foremost, I would like to express my sincerest gratitude to my advisor, Cecily Wolfe, for tutoring me in the art of doing science. I could not have asked for someone more dedicated and supportive. I thank her for her consistent encouragement, understanding and advice, and for awakening the scientist in me. I am also deeply grateful to my committee members Rob Dunn and Fred Duennebier for their support, enthusiasm and constructive reviews. Special thanks go to Carolyn Parcheta for helping me pick uncountable earthquake arrivals. On a personal note, my appreciation goes to my fellow students and friends Darwina Griffin and Kelly Mitchell for brightening my days with their humor. “Muchas Gracias” to my family and friends for reminding me that distance is relative: I am just a phone call away. I am particularly indebted to my better half, Jorge, for his love and patience during those times when there was no light at the end of anything and whose creative endeavors allowed me to maintain my (in)sanity throughout the writing of this thesis.

ABSTRACT

Data recorded by the Plume-Lithosphere Undersea Melt Experiment (PLUME) during a deployment of two successive networks of ocean-bottom seismometers (OBSs) around the Hawaiian Islands were analyzed to characterize seismicity in the island chain. Hypocentral estimates for 1,147 microearthquakes were determined in this study and a total of 2,894 events were associated with earthquakes already in the USGS Hawaiian Volcano Observatory (HVO) internal catalog. Analyses indicate that earthquake detection rates are increased when seismograms are high-pass filtered above about 5 Hz to reduce the seismic noise from wind-generated waves. The PLUME earthquake spatial patterns are substantially different than the patterns of earthquakes located by the HVO network. Diffuse seismicity was found in the offshore region to the southeast of the island Hawaii, as well as clusters of earthquakes west of Hawaii. Microearthquakes are found to be more common in the Maui and Molokai region, than previously realized; many of these locate in the mantle. Only a small number of offshore microearthquakes are found to occur near Oahu, Kauai and Niihau. Events occurring in these regions may reflect the stresses associated with volcano loading and plate flexure. On the time scale of earthquake recurrence, the 2-year PLUME recording period was quite short, but during this time interval the Molokai Fracture Zone was not seismically active, and no evidence of a hypothesized “Diamond Head Fault” was found.

TABLE OF CONTENTS

LIST OF TABLES

Table **Page**

LIST OF FIGURES

1. INTRODUCTION

The Hawaiian Islands are located in a geologically complex and seismically hazardous setting. According to the United States Geological Survey Hawaiian Volcano Observatory (HVO) earthquake catalog and studies such as *Wyss and Koyanagi* [1992], and *Klein and Wright* [2000] the entire island chain is marked by significant and continuous small magnitude seismic activity as well as by less frequent large damaging earthquakes.

For almost a hundred years, HVO has conducted the continuous instrumental recording of earthquakes in Hawaii. Each year its staff analyzes and locates thousands of earthquakes that occur beneath the islands, recorded on the HVO seismic network of mostly short-period seismometers. The first seismic monitoring instruments were installed in Hawaii around 1912 [*Klein and Wright*, 2000] but it was not until 1959 under the guidance of Jerry Eaton that the era of high quality seismometer coverage began, proving more accurate earthquake locations and depths, as well as possible source mechanisms and magnitudes. Prior to 1959, much of our knowledge of earthquakes came from historic patterns of damage and shaking. The combination and analyses of both historic and modern data have lead to much of the present understanding of Hawaii's earthquake hazards [*Wright and Klein*, 2000].

Since 1912, the short-period seismic network on the island of Hawaii has expanded to 48 stations [*Nakata and Okubo*, 2008]. The land-based network consists primarily of single-component 1-Hz geophones that are sensitive to local earthquakes and is designed to monitor volcano seismicity and tectonic earthquakes on the island of

Hawaii. HVO's network coverage is most dense on Kilauea Volcano and a sparser network of stations covers Mauna Loa and Hualalai. In 1999 HVO deployed three short-period instruments on Maui, yet these stations have not been operational for several years. Regardless of the fact that the seismicity data and seismic network have improved significantly, it is important to note that most of HVO seismic monitoring has been focused on the Big Island of Hawaii.

Currently, HVO uses its stations on Hawaii to locate high-frequency earthquakes and it also receives and uses data from two seismometers located on the islands of Maui and Oahu, operated by the Pacific Tsunami Warning Center [e.g., *Nakata and Okubo*, 2008]. There is an ongoing effort to expand station coverage on all of the major islands and to upgrade the network to include seismometers that are capable of recording a much wider range of seismic signals. This effort will eventually complete a Hawaii Integrated Seismic Network lead by the Pacific Tsunami Warning Center and the USGS [*Shiro et al*., 2006].

While HVO is able to record some offshore seismicity, such as the 1996 Loihi swarm [*Caplan-Auerbach and Duennebier*, 2001], the detection and location of small magnitude offshore seismic activity is limited by the fact that there are no seafloor seismometers and instrumental coverage is very sparse on the islands outside of Hawaii. The geometry of the island chain also plays an important role, since it restricts the network aperture to a nearly linear shape that is not optimal for location of submarine earthquakes. Most of the earthquakes that occur farther than 50 km offshore can only be recorded by HVO if they are magnitude 3-4 or larger [*Wyss and Koyanagi*, 1992; *Klein et al.*, 2001]. Similarly, these seismic events are often too small in size to be detected

teleseismically by global stations. These limitations on Hawaii's seismic recording have long challenged our understanding of island tectonics.

In addition to the thousands of microearthquakes that the island of Hawaii experiences each year, the islands of Maui and Oahu are also seismically active: large historic earthquakes are known to have occurred in this area (Figure 1) and earthquakes with $M_L > \sim 3$ are occasionally detected by modern instrumentation [cf. *Klein et al.*, 2001, Figure 2]. The location and analyses of large earthquakes near the islands of Maui, Lanai, Molokai and Oahu have also been conducted using historical records and patterns of felt intensities [e.g. *Cox*, 1986b; *Furumoto et al.*, 1990; *Wyss and Koyanagi*, 1992; *Wright and Klein*, 2000]. In most cases such interpretations were made using a limited amount of data with uncertain accuracy. Despite these attempts to characterize seismicity in regions north of the island of Hawaii, little is known about the recurrence and spatial distribution of large historic earthquakes. Similarly, we have little knowledge of the ongoing microearthquake activity outside the Big Island of Hawaii.

Studies of the seismic history of the Maui-Oahu region over the past decades have concluded that the seismic risk to the islands of Maui, Molokai, Lanai, Kahoolawe, and Oahu is not negligible [*Wright and Klein*, 2000; *Klein et al.*, 2001]. For example, since 1868, approximately 43 strong earthquakes of magnitude 6 or greater have occurred on Hawaii Island and about 8 events of magnitude 6 or larger have occurred in the vicinity of the islands of Maui and Molokai (Figure 1). However, there are still uncertainties in the locations of the three most damaging events that took place in that region. The 1871 Lanai earthquake with an estimated magnitude ~6.8 was one such event. Some researchers [e.g., *Furumoto et al*., 1973; *Cox*, 1985] argue that this earthquake was

located near the island of Lanai, but *Klein and Wright* [2000] suggest it was located further northward in the Molokai region. The 1871 earthquake generated maximum Modified Mercalli Intensities (MMI) of up to VII [*Wyss and Koyanagi*, 1992] and was responsible for producing the most severe earthquake damage on record on the island of Oahu [*Cox*, 1985]. Similarly, another magnitude ~6.8 earthquake in 1938 occurred in the offshore region northeast of Maui [*Holman*, 1982; *Wyss and Koyanagi*, 1992] and was felt throughout the Hawaiian Island, causing significant damage on Maui (MMI VIII), Molokai, Lanai and Oahu (MMI V-VI). The approximate locations of the 1871 and 1938 earthquakes are indicated in Figure 1. Another event of interest is the 1948 Oahu earthquake of estimated magnitude ~4.8. This event is not displayed in Figure 1, but it produced damage mainly to the city of Honolulu (maximum MMI VI) and therefore its epicenter is inferred to be close to the island of Oahu [*Cox*, 1986a]. To date, its exact location is unclear.

Wyss and Koyanagi [1992] state that both the 1871 and the 1938 earthquakes fit the isoseismal gradient patterns typical for earthquakes of crustal depths (< ~15 km), but the felt areas seem large compared to other Hawaiian earthquakes of similar magnitudes, perhaps indicating that these two earthquakes occurred on deeper, mantle fault zones. Significant microseismicity and mantle earthquakes are known to occur in the mantle around Hawaii [c.f. *Wolfe et al.*, 2004]. The 1973 M_W 6.2 Honomu earthquake occurred beneath the Hamakua Coast of the Big Island at 40 km depth [*Unger and Ward*, 1979] and the 2006 Mw 6.7 Kiholo Bay earthquake was located at 39 km depth [*Yamada et al.*, submitted]. Such mantle earthquakes have been proposed to reflect the stresses generated

by the growing volcanoes, the flexure of the lithosphere and gravitational adjustment of the volcanic edifice [*Pritchard et al.*, 2007; *McGovern*, 2007].

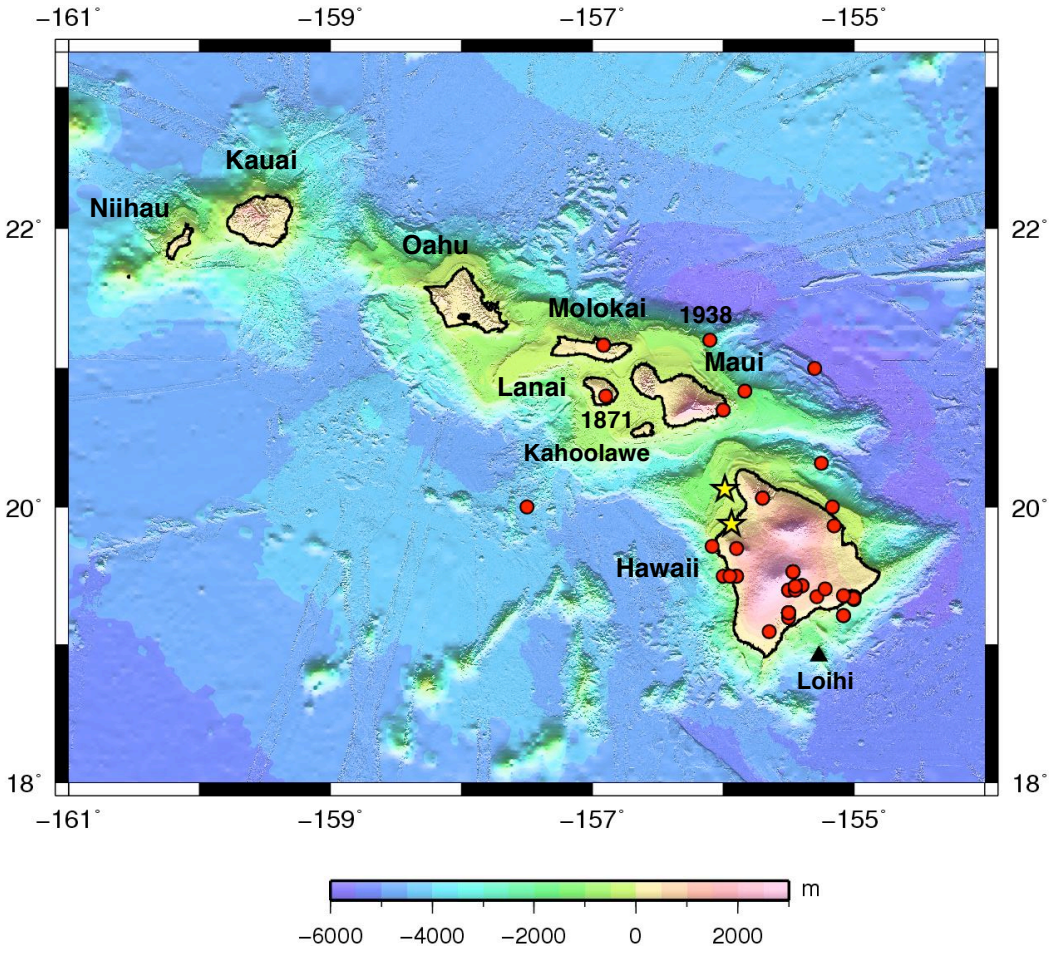

Figure 1. Bathymetry and topography of Hawaii showing the location of the major islands and large (M≥6) earthquakes. Black triangle shows the location of Loihi Seamount. Red circles represent the epicenters of the large historical (1823-2008) Hawaiian earthquakes. Yellow stars indicate the 2006 M_W 6.7 Kiholo Bay earthquake and its M_W 6.0 Mahukona aftershock. Locations were compiled from historic and instrumental sources by *Klein and Wright* [2000] and the United States Geological Survey (USGS) earthquake catalog. The 1871 Lanai earthquake and the 1938 Maui earthquake are also identified.

It has been argued that tectonic activity capable of generating hazardous earthquakes in the region Maui-Oahu is related to seafloor fractures and suspected faults around the islands. Some studies have speculated that the Molokai Fracture Zone (or MFZ), extending westward from North America and intersecting the Hawaiian Islands (Figure 2), is the site of past strong earthquakes with the potential for generating major earthquakes in the future [*Furumoto et al.*, 1973; *Mullineaux et al.*, 1987]. Because this fracture zone is tectonic in origin, generated 70-80 Myr ago [*Müller et al.*, 1997] by oceanic transform faulting, it has been suspected to be a preexisting zone of weakness where faulting might preferentially occur and contribute to the regional Hawaiian seismicity. However, past earthquake locations have been too poor to validate these speculations.

Similarly, the existence of a "Diamond Head Fault" [*Estill*, 1979; *Furumoto et al.*, 1980; *Cox*, 1986a] has been suggested based on prior analyses of a small temporary OBS deployment (Figure 2). If real, this hypothesized fault might cause damaging earthquakes near the island of Oahu and more specifically near the city of Honolulu. Due to the limited extent of prior seismic monitoring, very little is known about these and other possible offshore faults.

While large earthquakes have large recurrence intervals, the recording of much more frequent offshore microseismicity may allow a better characterization of the distribution and rate of Hawaiian earthquakes and therefore contribute to our understanding of Hawaii's offshore hazards, clarifying some conjectures about Hawaii's fault zones.

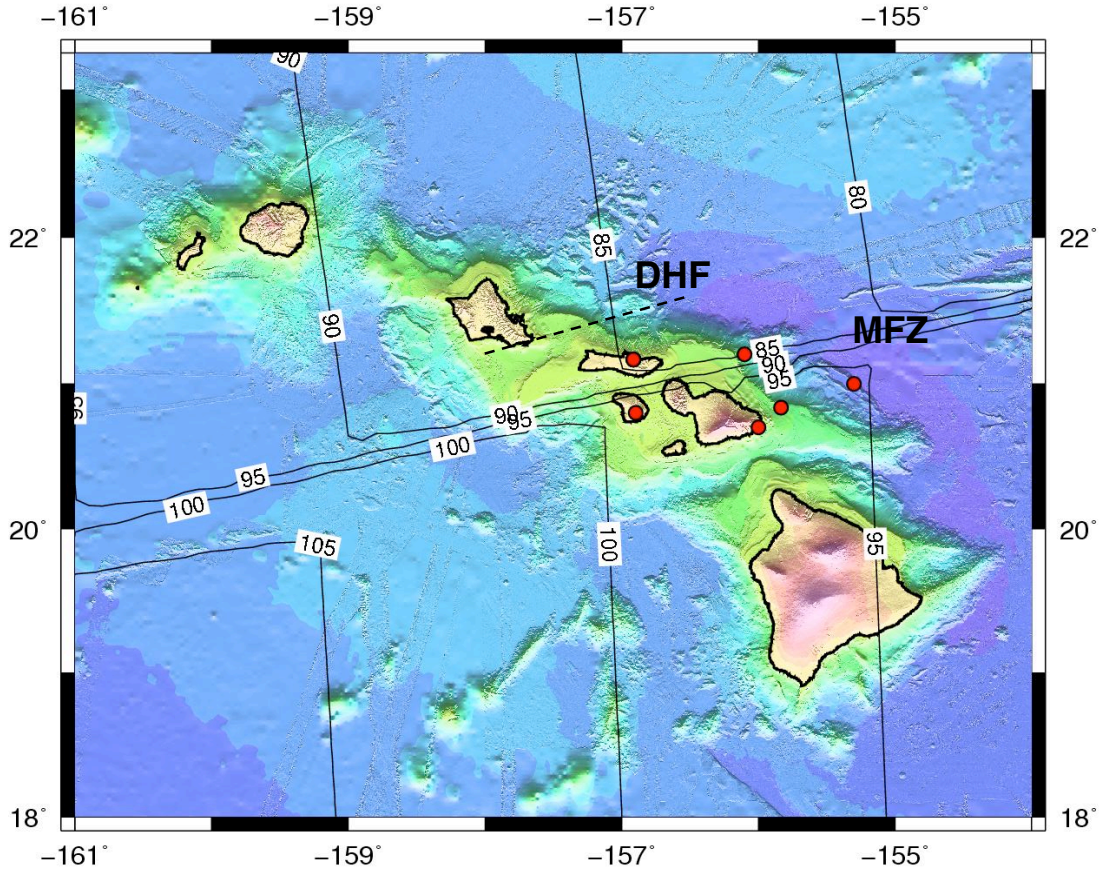

Figure 2. Location of the Molokai Fracture Zone (MFZ) and the Diamond Head Fault (DHF). The epicenters of six large (M≥6) historic earthquakes are displayed as red circles. Black solid lines represent isochrons of the seafloor around the islands of Hawaii from *Müller et al.* [1997]. Contours indicate ocean floor age in millions of years (Ma). The location of the east-west striking Molokai Fracture Zone is indicated by an offset in seafloor ages that runs throughout the islands of Molokai, Maui and Lanai. The location of a speculated Diamond Head Fault is shown as a dashed black line based on *Estill* (1979) and *Cox* (1986a).

Klein et al. [2001] used a limited catalog dating back to 1868 to prepare the probabilistic maps of peak ground acceleration along the main Hawaiian Islands. These maps display the seismic hazard or the probabilistic distribution of earthquake shaking levels that can be expected in the region. Seismic hazard assessments are attempts to

quantify the likely future seismic activity rates and strengths, based on knowledge of the past and present [*Stein and Wysession*, 2003]. The maps provide detailed information to assist engineers in designing structures that will withstand shaking from earthquakes. *Klein et al.* [2001] found that the seismic hazard for the state of Hawaii is the highest along the southeast coast of the Big Island, where damaging earthquakes tend to occur on a detachment fault between the preexisting oceanic crust and the overlying volcano [*Lipman et al.*, 1985], partly driven by the stresses associated with dike intrusion in the rift zones [e.g. *Owen et al.*, 2000]. Such events include the 1823 "Hawaii's first known" earthquake (M_I = 7.2), the 1868 (~M_I = 7.9) and the 1975 Kalapana earthquake (M_W = 7.7). *Klein et al.* [2001] estimated that the second highest hazard occurs along the Kona coast of the Big Island, where it is believed that the Kealakekua fault zone acts as a similar type of detachment [e.g., *Wolfe et al.*, 2004]. This feature appears to be the source of the 1951 Kona earthquake (M=6.9) [*Beiser et al.*, 1994]. The seismic hazard, as determined by *Klein et al.* [2001], decreases exponentially toward the northwest of Hawaii.

While "earthquake hazard" is certainly highest on the island of Hawaii, it is "earthquake risk" that reflects the potential economic and social costs. Earthquake risk is the danger that hazard poses to life and property. It reflects both the hazard and the exposure to the hazard factors, as for example population density (highest on Oahu), and building quality. *Wright and Klein* [2000] proposed that two of the most devastating geologic events that could potentially cause societal damage and disruption today are: a Mauna Loa southwest rift eruption and a large earthquake near Maui. The earthquake risk for highly populated cities like Honolulu is still very hard to judge because of the poor

knowledge of the hazard level due to the short history of known earthquakes. Nevertheless, many have proposed that another event similar to those in 1871 or 1938 would result in significant damage to cities and towns on Maui and Oahu. For example, the Pacific Disaster Center, working with the Hawaii State Civil Defense and the Hawaii State Earthquake Advisory Committee, developed a Hawaii HAZUS (Hazards U.S.) atlas to calculate expected damage from potential future earthquakes. Their work estimated that a magnitude 6.7-7.0 earthquake in the Lanai or Maui region would produce $1 billion in damage if it occurred in present time and would cause a number of casualties [see *http://www.pdc.org/hha/html/hzshome.jsp*].

In 2005-2006 and again in 2006-2007, the Plume-Lithosphere Undersea Melt Experiment (PLUME) deployed two consecutive networks of ocean bottom seismometers (OBSs) around the islands of Hawaii. Continuous seismic data recorded by the two different OBS arrays and several land stations during the 2-year period provide a rare opportunity to characterize onshore and offshore microseismicity at Hawaii. This thesis presents analyses of the local seismicity recorded by PLUME and the relationship of local seismicity to tectonic and volcanic activity. These data are used to examine and address some of the previous assumptions about the characteristics of fault zones around the Hawaiian Islands. The results are utilized to provide a new and enhanced view of seismicity along the major islands and reveal new patterns of seismic activity.

2. EXPERIMENT SETTING

The Plume-Lithosphere Undersea Melt Experiment, or PLUME, was a 2-year (2005-2007) deployment of broadband ocean bottom seismographs (OBSs) along the Hawaiian Islands. The Scripps Institution of Oceanography (SIO), the Woods Hole Oceanographic Institution (WHOI), the University of Hawaii, the Yale University, and the Carnegie Institution of Washington conducted this project in order to collect data that can resolve the mantle seismic structure beneath the Hawaiian hotspot and swell. A major objective was to construct a three-dimensional image of a hypothesized upwelling plume in the mantle beneath Hawaii, and to determine its location, its width, and the magnitude of the thermal anomaly associated with it [*Laske et al.*, submitted].

The experiment was divided into two consecutive year-long OBS deployments to obtain optimal coverage. The first OBS array (PLUME1) was deployed in 2005. Thirty five stations were deployed at a spacing of 75 km around the island of Hawaii (Figure 3, Table 1). This OBS array was designed to resolve the presence of a possible mantle plume and to image its shape and the magnitude of the seismic anomaly. A second OBS deployment (PLUME2) was launched in 2006 with wider spacing. Thirty eight stations were spaced about 200 km apart (see Figure 3, Table 2). This configuration was designed to allow a detailed study of the Hawaiian Swell and to extend the depth resolution of body wave imaging down through the mantle transition zone and into the lower mantle [*Laske et al.*, submitted]. PLUME was a passive seismic experiment, where instruments were emplaced on the seafloor to record earthquake-generated seismic waves traveling through a potential mantle plume. In this type of experiment, signals (body and surface

waves) from remote large earthquakes are collected and used to infer mantle heterogeneity [*Laske et al.*, submitted; *Collins*, 2004].

The OBSs from the U.S. National Ocean Bottom Seismograph Instrument Pool (OBSIP) were used in PLUME. Each instrument had a broadband three-component seismometer and a differential pressure gauge (DPG). The OBS network consisted of WHOI instruments (Guralp CMG-3T sensors) and SIO OBSs (Nanometrics Trillium 40 sensors on the first deployment and Trillium 240 sensors on the second deployment). Data were recorded continuously in the range of 32.5-40 samples per second (sps), although a subset of instruments on the first deployment were erroneously set to 125 sps.

Concurrently a network of ten temporary land stations from the Carnegie Institution of Washington was also deployed at strategic places along the islands of Hawaii (Figure 3, Table 3). These seismometers were broadband (Streckeisen STS-2 sensor), three-component and collected continuous data at a sampling rate of 20 sps.

All the OBS locations were determined with detailed acoustic interrogation after deployment. The instruments were also synchronized with GPS clocks before deployment and after retrieval and corrected for the effects of clock drift and for the leap second addition at the end of 2005. The number of PLUME stations providing useable data (shown in Figure 3) was significantly reduced, especially on the second deployment, due to malfunctioning or lost instruments, producing a diminution of instrument coverage northeast of the island of Hawaii. A total of ten OBSs were lost during the second deployment; however, two of them were subsequently recovered by a later OBS recovery cruise with the WHOI JASON ROV [*Laske et al.*, submitted].

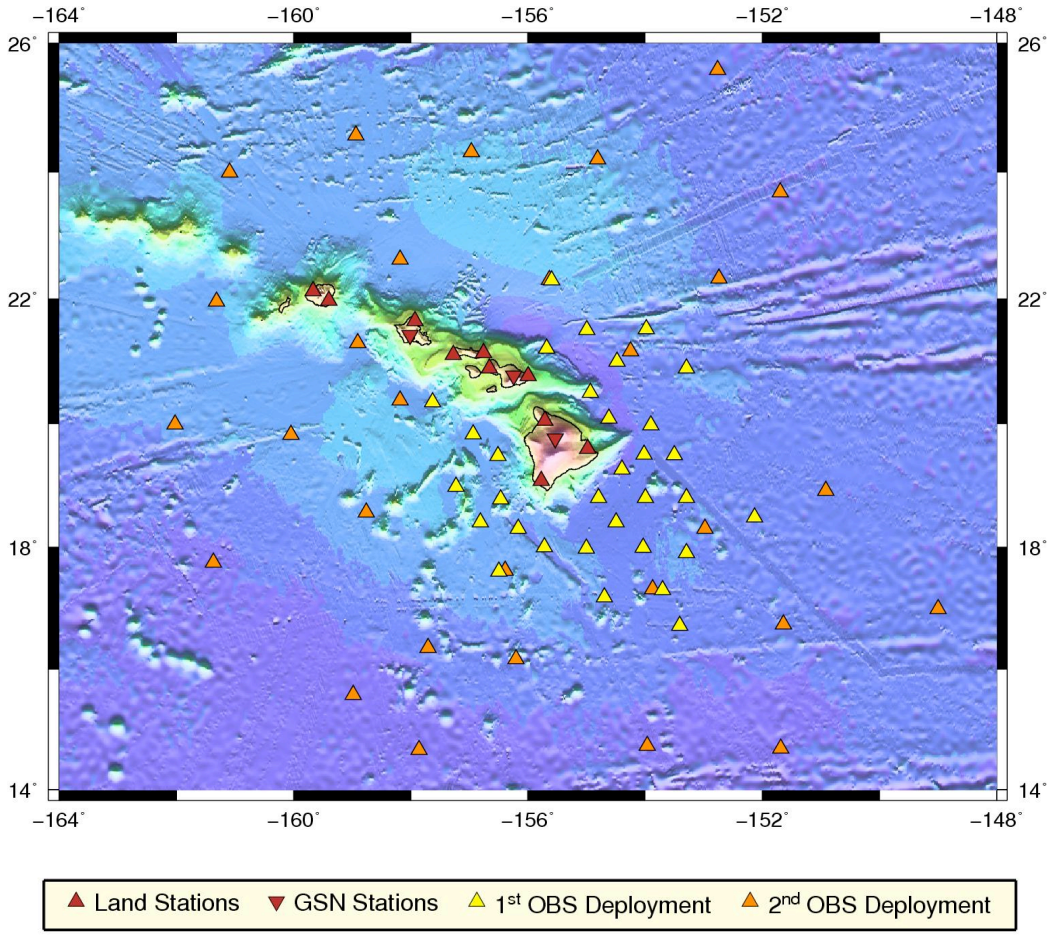

Figure 3. Location of PLUME instruments. The project was divided into two deployments of broadband ocean bottom seismometers (OBSs) and a deployment of land seismometers. The first OBS deployment (2005-2006) is indicated by yellow triangles, 35 stations were placed at a spacing of 75 km around the Island of Hawaii with a total aperture of 500 km. Orange triangles represent the second OBS deployment (2006-2007), the spacing between the 38 deployed stations is 200 km with an aperture of 1000 km. Only stations that recovered data are shown. Both deployments collected data continuously for a year. PLUME land stations are shown as red triangles; also shown as inverted red triangles are the sites of permanent stations KIP (on Oahu), POHA (on Hawaii), and MAUI (on Maui), from the Global Seismic Network (GSN).

Table 1. Station information for the PLUME first OBS deployment

Station	Latitude, °N	Longitude, °W	Depth, m
PL24	18.8031	-154.7974	-5319
PL27	18.0003	-155.7150	-5099
PL22	17.9884	-154.0305	-5057
PL13	19.2625	-154.3940	-5515
PL01	20.0889	-154.6178	-5580
PL34	19.8327	-156.9320	-4748
PL17	18.4814	-152.1324	-5184
PL07	21.5197	-153.9827	-4912
PL23	18.4017	-154.4959	-5167
PL02	20.4999	-154.9375	-5065
PL30	18.3010	-156.1670	-5091
PL15	18.8009	-153.2959	-5077
PL35	20.3461	-157.6276	-4650
PL08	20.8926	-153.2920	-5159
PL10	19.9791	-153.9024	-5336
PL03	21.2055	-155.6794	-5144
PL11	19.4952	-153.5032	-5181
PL14	18.7976	-153.9923	-5252
PL18	17.9062	-153.2906	-4938
PL20	17.2975	-153.7008	-5120
PL05	21.5070	-154.9944	-5196
PL29	18.4042	-156.8082	-4627
PL26	17.9757	-155.0026	-4997
PL33	19.4777	-156.5101	-4707
PL31	18.7750	-156.4651	-4610
PL04	22.2936	-155.5947	-4515
PL06	21.0000	-154.4828	-5373
PL12	19.5022	-154.0150	-5385
PL19	16.7119	-153.4067	-5163
PL21	17.1803	-154.6925	-4993
PL28	17.6028	-156.4995	-4792
PL32	18.9831	-157.2286	-4604

Table 2. Station information for the PLUME second OBS deployment

Station	Latitude, °N	Longitude, °W	Depth, m
PL41	24.5738	-158.9331	-4749
PL45	24.2006	-154.812	-4686
PL37	19.8234	-160.0475	-4676
PL74	20.3778	-158.1795	-4541
PL50	22.3199	-152.7427	-5021
PL59	16.9890	-149.0009	-5374
PL68	14.6596	-157.8591	-5637
PL46	24.3121	-156.9646	-4428
PL65	17.3154	-153.8682	-5115
PL62	14.6891	-151.6866	-5765
PL57	18.9142	-150.915	-5335
PL61	16.7378	-151.6376	-5186
PL71	17.7469	-161.3676	-5601
PL51	23.6843	-151.6957	-5485
PL39	21.9563	-161.3149	-4543
PL55	18.3018	-152.9812	-5076
PL36	21.2984	-158.903	-4762
PL48	22.2999	-155.6362	-4528
PL69	16.3484	-157.7008	-5365
PL44	25.5928	-152.7658	-5420
PL66	17.6149	-156.3877	-4826
PL43	26.7767	-155.7653	-5545
PL35	19.9885	-162.0245	-4897
PL40	23.9931	-161.0931	-4691
PL47	22.6217	-158.1842	-4830
PL49	21.1669	-154.2492	-5173
PL63	14.7311	-153.9655	-5603
PL67	16.1630	-156.207	-5112
PL70	15.5734	-158.9809	-5591
PL73	18.5631	-158.7602	-4686

Table 3. PLUME land stations and GSN stations* used in this study

Station	Latitude, °N	Longitude, °W	Depth, m
BIG2	19.0790	155.7730	582
BYUH	21.6460	157.9310	23
CCHM	20.7710	155.9970	60
DLAH	19.6010	154.9830	52
HPAH	20.0460	155.7110	775
KCCH	21.9710	159.4010	128
KIP*	21.4233	158.0150	70
LHSM	20.8910	156.6580	204
MAUI*	20.7668	156.2448	2060
MRKH	21.1090	157.2700	143
NGOK	22.1230	159.6650	1157
PHRM	21.1360	156.7560	407
POHA*	19.7575	155.5325	1967

PLUME is the first large-scale, modern broadband OBS network deployed around the islands. Although the PLUME experiment was designed to achieve specific seismic imaging goals, these data can be also utilized to locate and characterize Hawaiian earthquakes, since stations recorded numerous local events during the year-long deployments. The dataset recorded by the PLUME deployments presented a unique opportunity to study microseismicity in Hawaii, which is the main purpose of this thesis.

3. DATA ANALYSIS

3.1. Event Detection

The data utilized represent just over two years of seismic recording and were analyzed using Antelope software developed by Boulder Real Time Technologies. PLUME OBS and land seismic data were incorporated into an Antelope database that also included waveform data from IRIS GSN permanent stations POHA and KIP (on Oahu) as well as GEOFON station MAUI (on Maui).

The first step in the data analysis involved running *dbdetect*, Antelope's automated detection algorithm. *Dbdetect* scans the waveforms and uses a standard Short Term Average and Long Term Average, STA/LTA, detector to identify possible earthquake-generated signals in the seismometer data. The detection technique compares a time-averaged ratio to a threshold value. For each variable under consideration, this method calculates a short-term mean, STA (a running average of the last few readings), and a long-term mean, LTA (a running average covering a longer period of time). STAs are sensitive to rapid increases in the amplitude of a time series and LTAs measure the local background amplitude. The ratio between the STA and LTA is compared to a specified threshold value or STA/LTA threshold. Thus the ratio of the STA to the preceding LTA is a measure of the local signal-to-noise. If the ratio is higher than a threshold value a phase arrival is declared.

Early in the analyses, it was found that the detection of microearthquakes (M_L < ~1.5-3) was highly dependent on the data filtering and was most successful when the waveforms were high pass filtered above 5 Hz. Nonetheless, multiple frequency

bands were analyzed, including 1-3 Hz, where most long-period (LP) earthquakes are usually identified. However, no such LP events were noticed and the data appear to be dominated by high frequency earthquakes.

It has been long known that the noise characteristics of ocean floor sites are different from continental sites, since ocean waves are an important source of seismic noise. Wind-generated waves represent the most important source of noise within the ocean at seismic frequencies [*Webb*, 1998] and Hawaii is not an exception. *Collins et al.* [2001] conducted an ocean-bottom seismic experiment southwest of the island of Oahu to estimate the effects of ambient noise on the quality of broadband seismic data. Their findings suggest that seismic instruments sitting on the seafloor record noisier data than on-land stations, especially in the frequency band between 0.1-5 Hz. Given that prior seafloor studies find that noise decays rapidly at higher frequencies, the improvement in microearthquake detection at high frequencies (> 5 Hz) likely reflects an improvement in signal-to-noise via a reduction in background noise levels.

Preliminary evaluation of the data also showed that the differential pressure gauge (DPG) data were noisier than seismometer data at high frequencies, leading to fewer detected events. A small number of T-phase arrivals were observed on the hydrophones: for example, both the DPG and seismometer detected an earthquake swarm at Loihi seamount in December 2005 and also a lava bench collapse into the ocean in November 2005. Based on this initial examination of the data, the DPG data were not included in the study of high-frequency earthquakes. Therefore, the analyses described in the next sections concentrate on the seismometer data.

3.2. Earthquake Location

This study focused on identification of local events, for that reason, teleseismic events were eliminated by matching them with events in global seismic catalogs. Earthquakes detected on the PLUME network were also compared to the list of events in the HVO internal earthquake catalog. This catalog was incorporated into an Antelope database and allowed the association of events detected by PLUME with those earthquakes already located by HVO.

The numerous event detections from *dbdetect* were automatically processed by the Antelope routine *dbgrassoc* to associate potential event locations and arrival phases to the detections. The program searches over pre-defined spatial grids for a candidate hypocenter that predicts arrival time moveouts to different stations that match the observations. To avoid numerous false associations, a requirement was set that candidate events from *dbgrassoc* contain picks from a minimum of five stations.

After the earthquake identification algorithms determined automated locations for the events, *P* and *S* arrival time picks were manually verified and refined using *dbloc2*, Antelope's interactive arrival time picking and location package, and a final hypocenter was derived. Figure 4 shows typical waveforms of PLUME OBS stations from a M_L= 2.1 earthquake beneath the island of Maui, with data filtered above 5 Hz. The seismograms of stations at varying distances show how seismic phases are identifiable, even for instruments placed ~260 km away from the epicenter. *P* and *S* wave arrivals are clear and distinguishable on the records of stations closer to the source, whereas, *S* waves tend to be the only prominent phase at distant stations. *P* wave arrivals were manually picked only on vertical channels, and *S* waves only on one of the horizontal channels.

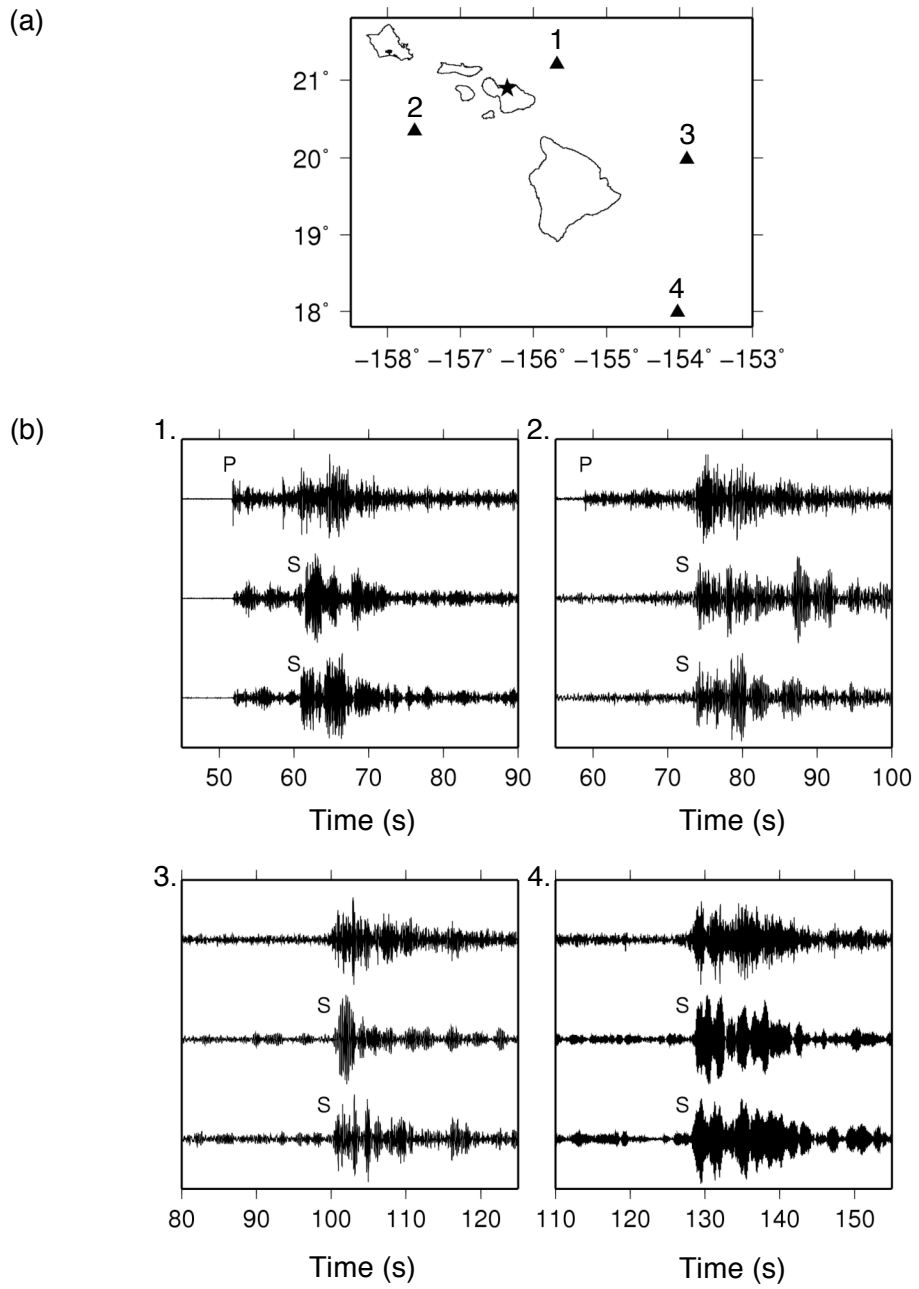

Figure 4. Examples of local microearthquake data. (a) Map showing the location of a M_L 2.1 earthquake (star) that occurred beneath Maui. Four stations (triangles) are shown that recorded the event at different distances. (b) Waveforms on the vertical (top seismogram) and two horizontal (bottom two seismograms) channels. Data are high-pass filtered above 5 Hz. For plotting, each seismogram is scaled by its maximum amplitude. Distinct phase arrivals are labeled on each seismogram. Note that *P* waves can only be picked at close stations (1 and 2), but *S* waves can be picked at both close and distant stations (3 and 4).

For the best quality event recordings, it was possible to pick *P* and *S* arrivals with confidence to within 0.1 s certainty, although in more typical cases the picking errors were between 0.5-0.6 s.

Final earthquake locations were determined using *dbloc2* using a simplified, 1-dimensional velocity model. PLUME-derived locations were estimated only for the subset of earthquakes that could not be associated to events already in the HVO catalog. Each earthquake in this subset was located using a minimum of four clear *P* wave or *S* wave arrivals. Antelope offers two choices within the Gauss-Newton method (GNM) for the generalized inverse: the pseudoinverse and the Levenberg-Marquardt algorithm [*Pavlis et al.*, 2004]. For the purpose of this study the Levenberg-Marquardt method (LMM) was used as the approach to locate the microearthquakes [*Levenberg*, 1944; *Marquardt*, 1963].

The simplified 1-dimensional velocity model consists of two layers, representing a crust overlying a mantle half space. The first layer extends from 0 to 11 km depth below sea level and consists of *P*-wave and *S*-wave velocities of 6.27 km/s and 3.6 km/s, respectively. The second layer is located at 11 km depth below sea level with a *P*-wave velocity of 8.3 km/s and a *S*-wave velocity of 4.6 km/s. This simple parameterization was chosen because of Antelope's elevation correction capabilities [*Pavlis et al*., 2004]. The location-dependent elevation corrections are made using the velocity in the topmost layer and require that no stations be below the depth of the top layer. The deepest OBS is at 5.7 km depth (Table 1 and Table 2) and OBSs presumably are sited on ~6 km thick oceanic crust, and thus the approximation of crustal velocities down to 11 km depth below sea level is reasonable. These elevation corrections are more important for PLUME than in

typical land-based experiments, owing to the huge range of station elevations in the experiment (from –5765 km to +2060 km) (see Tables 1-3). For the interpretations presented in this paper, this approximate velocity model is considered to be adequate, although there is likely some tradeoff between velocity and absolute locations.

The crustal structure model of the island chain is described by *Zucca et al.* [1982] and *Watts and ten Brink* [1989]. These works report that the bottom of the flexed oceanic crust is at ~15 km depth beneath the major islands, although it may extend to deeper depths (~20 km) beneath the center of the Big Island of Hawaii. For the purpose of this study, earthquakes that locate at depths greater than 20 km will be referred as mantle earthquakes.

3.3. Location Uncertainties

The possible errors in earthquake locations were assessed using the results from Antelope's standard location analysis capabilities [*Pavlis et al*., 2004]. Figure 5 shows histograms from the 1st and 2nd PLUME deployments, respectively. These figures display histograms of the distribution of the standard arrival time error between the observed and calculated arrival times (STDOBS), as well the estimated lengths of the semi-major and semi-minor axes of the horizontal confidence ellipse (in kilometers) and the error in depth (at 68% confidence). This information is calculated by Antelope and stored in its *origerr* table, and reflects a linearized estimate of location errors estimated using the inversion covariance matrix. Such estimates should be considered a lower bound, as errors are likely much larger due to the fact that the earthquake location problem is nonlinear. Indeed, the ~0.5 s standard arrival time errors are 5-10 times greater than the

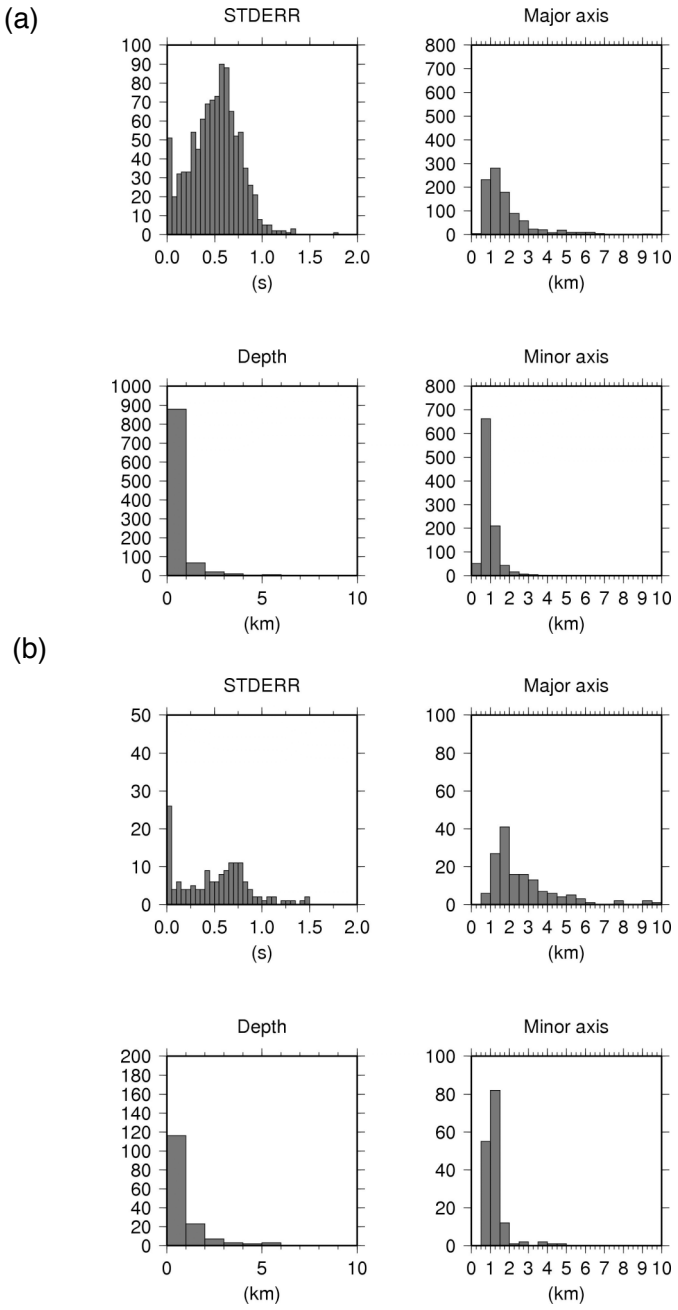

Figure 5. (a) Histograms of estimated errors for new earthquakes located on the 1st PLUME deployment. STDERR reflects the misfit in the arrival times of phases used to locate the event, defined by the square root of the time residuals divided by the number of degrees of freedom. Also plotted are the lengths of the semi-major and semi-minor horizontal confidence ellipses and the estimated errors in depth (at 68% confidence). (b) Histograms of estimated errors for new earthquakes located on the 2nd PLUME deployment. See Figure 5a for further information.

errors typically obtained with local seismic networks, indicating large picking errors and correspondingly large location errors. It is likely that location errors are thus larger than indicated in Figure 5.

The resolution of earthquake focal depths is likely variable across the PLUME earthquake catalog, as the depth quality for an individual event reflects the available station coverage and picking errors. For example, focal depth resolution is significantly better when an event is located inside a seismic network and when *P* and *S* wavedata are available within a distance of about one focal depth [e.g., *Duschenes et al*., 1983; *Wilcock and Toomey*, 1991]. For this reason, whenever possible both *P* and *S* waves were picked at the closest stations to an earthquake, although for distant stations *S*-waves were typically the only phase that was pickable.

3.4. Magnitude Calculation

Because most earthquakes only display good signal-to-noise ratios at frequencies higher than 5 Hz, earthquake magnitudes could not be estimated using Antelope's local magnitude (M_L) calculator, *dbml*. This calculator allows application of a Wood-Anderson filter to make the data compatible with the response of a ~1 Hz Wood-Anderson seismometer and its magnitude scale is calibrated for this limited frequency band. In order to estimate earthquake magnitudes at frequencies higher than 5 Hz, a new magnitude estimation function was constructed and calibrated to match the prior magnitudes provided by HVO. The earthquakes for which locations and magnitudes are determined by HVO (as listed in the Advanced National Seismic System, ANSS, catalog)

were selected as the calibration data set, yielding a total of 2,678 local earthquakes with prior estimated instrumental magnitudes.

The first step in creating a new magnitude algorithm consisted of calculating the total distance between detected earthquakes and instruments recording such events. This process was done for each earthquake in the PLUME database. Additionally, the wave amplitudes of the largest arrival (typically the *S* wave) recorded on the 5 Hz high-pass filtered seismograms were also measured. The measured maximum wave amplitude was corrected for nominal seismometer magnification and also a signal-to-noise cutoff was applied to remove poor signals by comparing arrival amplitudes with the amplitude of the noise prior to the *P*-wave arrival.

A plot of the logarithm of the amplitudes ($\log_{10}$ A) versus source-receiver distances was created and examined for each earthquake. It was found that these plots typically displayed a linear decay with distance. Therefore, a line was chosen to fit the log-amplitude versus distance data in the least-squares sense. Two assumptions were taken into consideration for the magnitude analysis in this study: 1) the intercept of the least-square line with the y-axis at zero distance is related to the magnitude or size of the event, and 2) the slope of the least-square line does not change and is the same for all earthquakes, which is equivalent to assuming that the influence of geometrical spreading and attenuation are the same for all events. Consequently, a single inversion was conducted for the values of intercept for each earthquake and for one value of slope**.**

Figure 6a shows the events selected to calibrate our magnitude scale. The earthquakes exhibit magnitudes spanning from 1 to 6.7, with the majority between 1 and 3. An earthquake-magnitude versus intercept relationship for the Islands of Hawaii was

then developed using these data (Figure 6a). A formula to convert measured intercepts to magnitudes was established using the simplest approach of fitting a least-squares line, as was shown in Figure 6a. Although the deviations from this line indicate uncertainties the order of ±0.5 magnitude units, this is not an unreasonable level of uncertainty for an M_L calculation. The relationship derived from the calibration dataset is:

$$M_{estimated} = \frac{(b - c)}{d}$$

M = estimated magnitude
b = value of measured intercept (a different value for each earthquake)
c = value of intercept with y-axis of line fit through the calibration dataset
d = value of slope of line fit through the calibration dataset

This function was subsequently used to estimate the magnitudes of the subset of microearthquakes located by PLUME. The magnitudes of 1,295 local microearthquakes were determined and are shown in Figure 6b. A total of 1,147 of these events were only recorded by PLUME. The remaining 148 events were registered by PLUME and HVO but these events were not reported in the ANSS catalog. The histogram plotted on Figure 6b indicates that the magnitudes of the new earthquakes detected by PLUME range from 0.5 to 3.5.

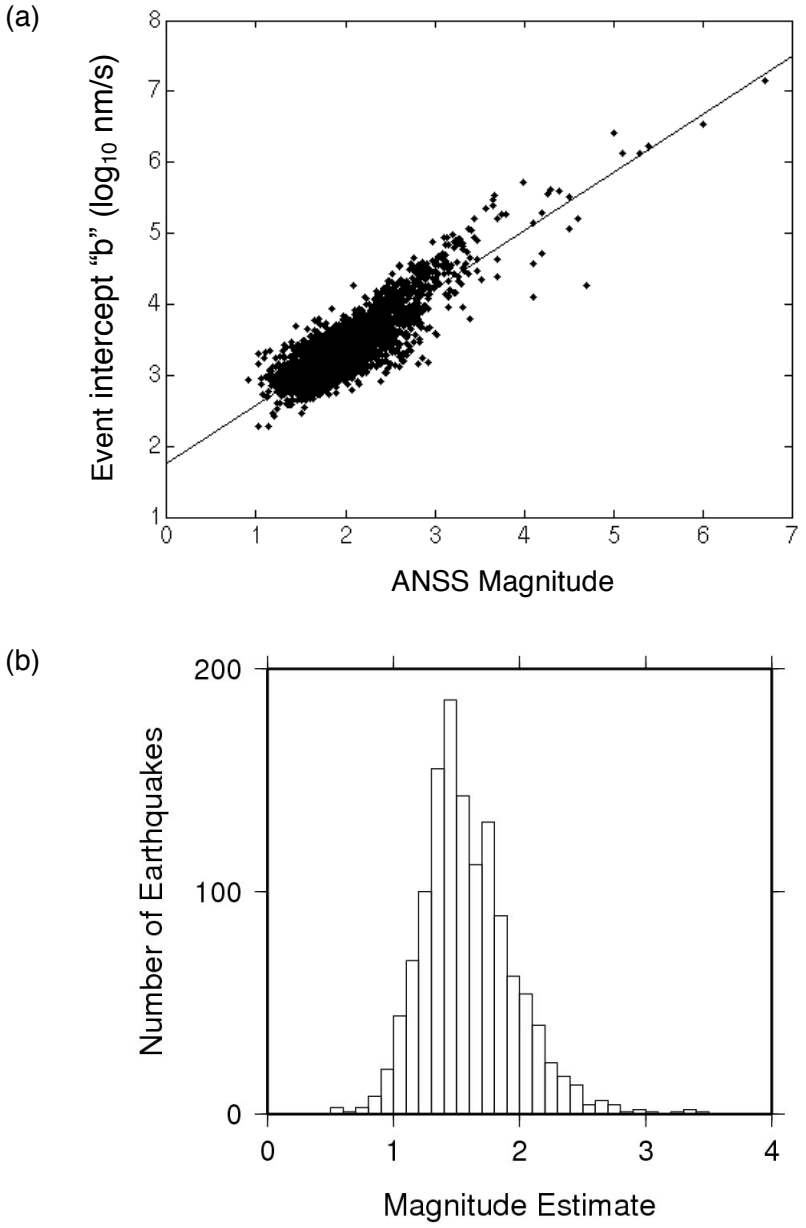

Figure 6. Magnitude Estimation. (a) Subset of earthquakes (black diamonds) used in magnitude calibration. These earthquakes were detected on PLUME deployments and associated to the HVO catalog. Horizontal axis displays the USGS ANSS magnitude, vertical axis displays the estimated log10 amplitude adjusted to 0 km distance (event intercept) from PLUME data. A linear relationship between event intercept and ANSS magnitude is estimated by a least-square fit (black line). (b) Histogram of estimated local magnitudes for the new microearthquakes located with the PLUME dataset. Magnitude bins are equal to 0.1. Microearthquakes magnitudes range from 0.5 to 3.5.

4. RESULTS

4.1. Microearthquakes: Epicentral Locations and Magnitudes

Analyses of the PLUME deployments detected a total number of 4,041 earthquakes. Hypocentral estimates for 1,147 new microearthquakes were determined in this study and a total of 2,894 events were associated with earthquakes already in the HVO internal catalog (refer to Table 4 for details). A typical HVO annual earthquake catalog consist of more than 4,000 recorded and located seismic events [*Nakata*, 2007; *Nakata and Okubo*, 2008]. However, analyses of PLUME data only detected about 2,900 events during the two-year experiment, indicating that more than ~5,100 events were undetected by PLUME. This difference reflects the lower detection threshold of the HVO network for earthquakes beneath the Big Island of Hawaii when compared to PLUME OBS-based network.

Table 4. Total number of earthquakes recorded on PLUME deployments

Deployment	Number of earthquakes detected by PLUME and HVO	Number of earthquakes detected only by PLUME	Total number of earthquakes
PLUME 1	1795	998	2793
PLUME 2	1099	149	1248

The spatial patterns of earthquakes recorded by PLUME and HVO instruments are shown in a regional map in Figure 7a. A detailed view of the seismicity is shown in Figure 7b. It is important to note that earthquakes in the HVO catalog were not relocated in this study. The epicentral locations displayed in Figure 7 thus have been derived by HVO.

The epicenters of the HVO earthquakes detected on PLUME (Figure 7b) are mostly concentrated on and around the island of Hawaii. Only 21 (~0.7%) of the total recorded earthquakes were located in areas closer to the islands of Maui and Oahu or in latitudes greater than 20.5ºN.

During the PLUME deployments, several moderate-to-large events occurred near the Big Island. In May and then in July 2005 two moderate earthquakes (M_L 5.1 and M_W 5.1 respectively) took place in the mantle (> 20 km) beneath the south flank of Kilauea Volcano. Subsequently in December of that same year, Loihi seamount experienced a small earthquake swarm (~100 events in the ANSS catalog) that lasted approximately one day. Loihi seismicity is shown in Figure 7b as a small offshore cluster southeast of Hawaii (~18.8°N, 155°W). Also in July 2005, a shallow, M_W 5.3 earthquake occurred offshore to the northeast of Hawaii. The event and its aftershocks are shown in Figure 7b. The 2006 M_W 6.7 Kiholo Bay earthquake and its hundreds of aftershocks, including the M_W 6.0 Mahukona earthquake, are also shown. These events constitute the large cluster situated beneath the west coast and offshore of Hawaii in Figure 7b.

(a)

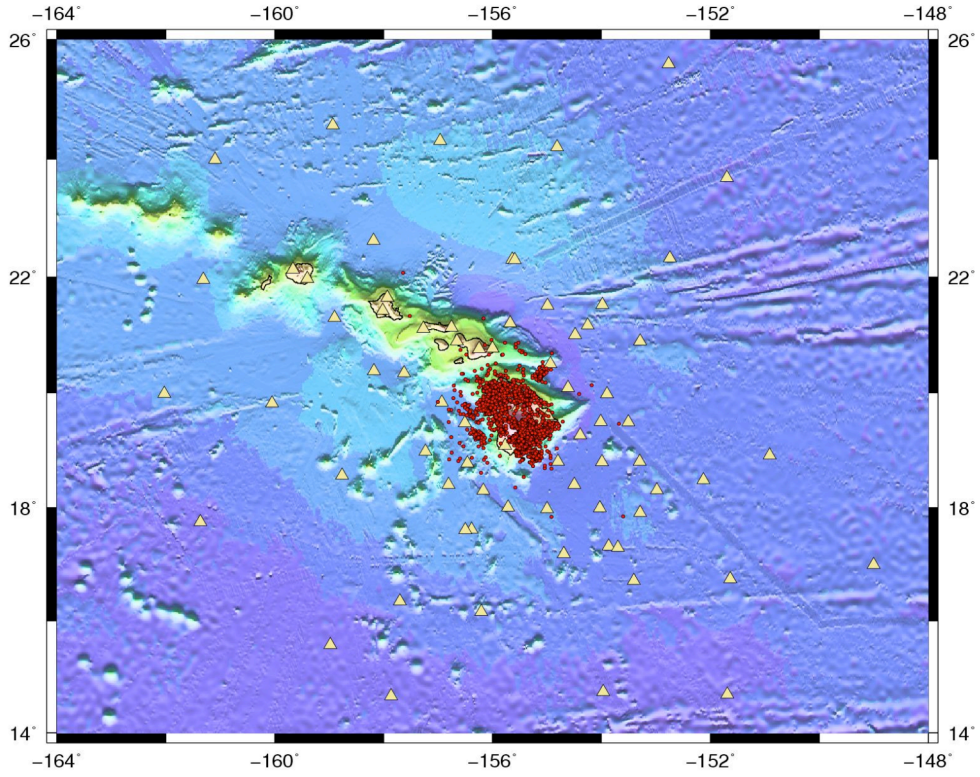

(b)

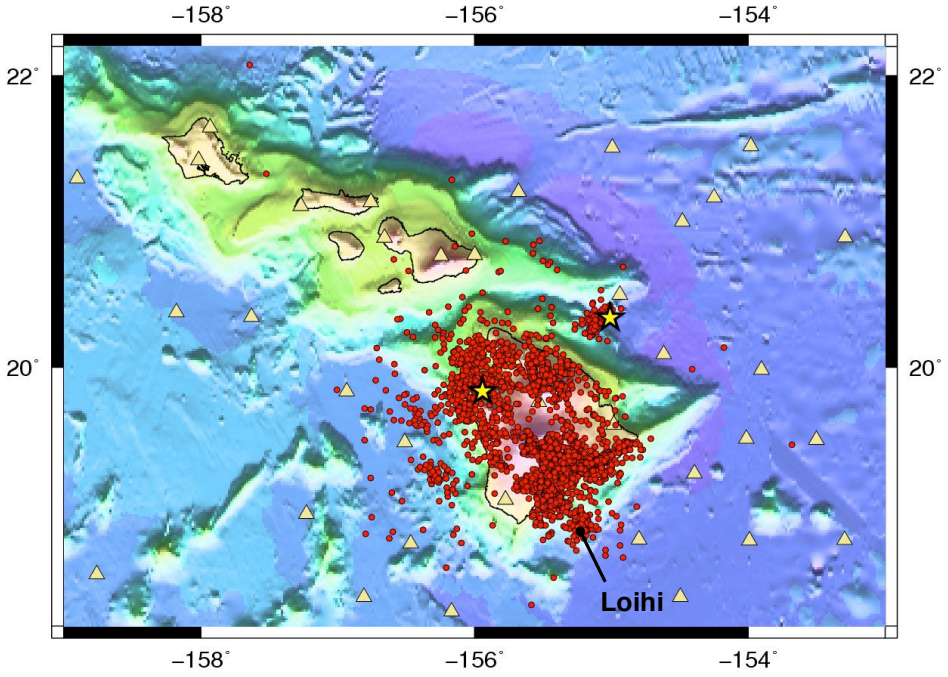

Figure 7. Epicenters of ~2,900 local earthquakes detected by PLUME instruments and also located by the HVO network. Epicentral locations are shown as red circles. PLUME stations are displayed as yellow triangles. Only stations that recovered data are shown. Global Seismic Network stations (POHA, KIP and MAUI) are also displayed. (a) Regional map. (b) Close-up view. Yellow stars represent the location of 2 moderate-to-large (MW > 5) earthquakes: a M_W 5.3 earthquake occurring in 2005 (right) and the 2006 M_W 6.7 Kiholo Bay earthquake (left).

Figure 8 shows 1,147 new events that were detected by the PLUME deployments but not by HVO. A total number of 183 events were located in regions with latitudes greater than 20.5ºN or around the islands of Maui, Molokai, Lanai, Oahu and Niihau. Approximately 964 events occurred near the Big Island or below latitude 20.5ºN. The PLUME network detected ~10 times more events in the Maui-Oahu-Niihau region than HVO. As expected, the improved geographic coverage by PLUME stations reduces the detection threshold in these areas.

PLUME data reveal significant, additional microseismicity to the northwest and offshore of the Big Island as shown in detail in Figure 8b. The spatial distribution of earthquakes contrasts with patterns shown by the HVO locations. The new seismicity, despite being dispersed overall, seems to localize in confined areas. Clusters of earthquakes are evident near the Big Island of Hawaii and also north of the islands of Maui and Molokai. Since this study seeks to provide an enhanced view of seismicity around the islands of Hawaii, the analyses that follow focused on discussing the characteristics of earthquakes detected only by PLUME (shown in Figure 8). The seismic activity has been sorted into regions: Hawaii, Maui-Molokai-Lanai and Oahu-Kauai-Niihau and it is described separately.

(a)

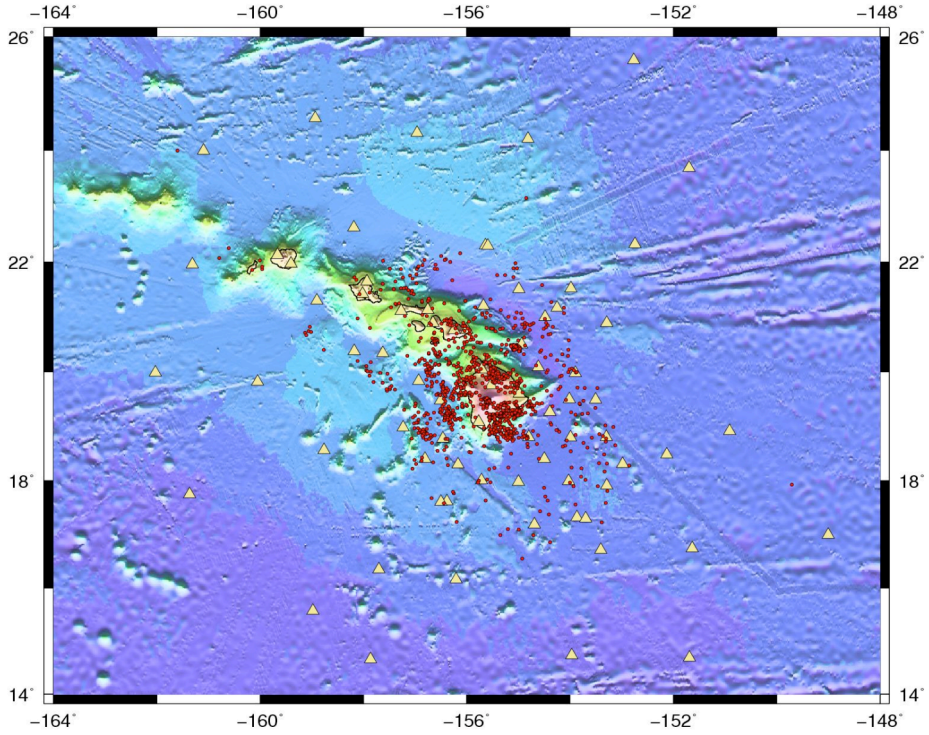

(b)

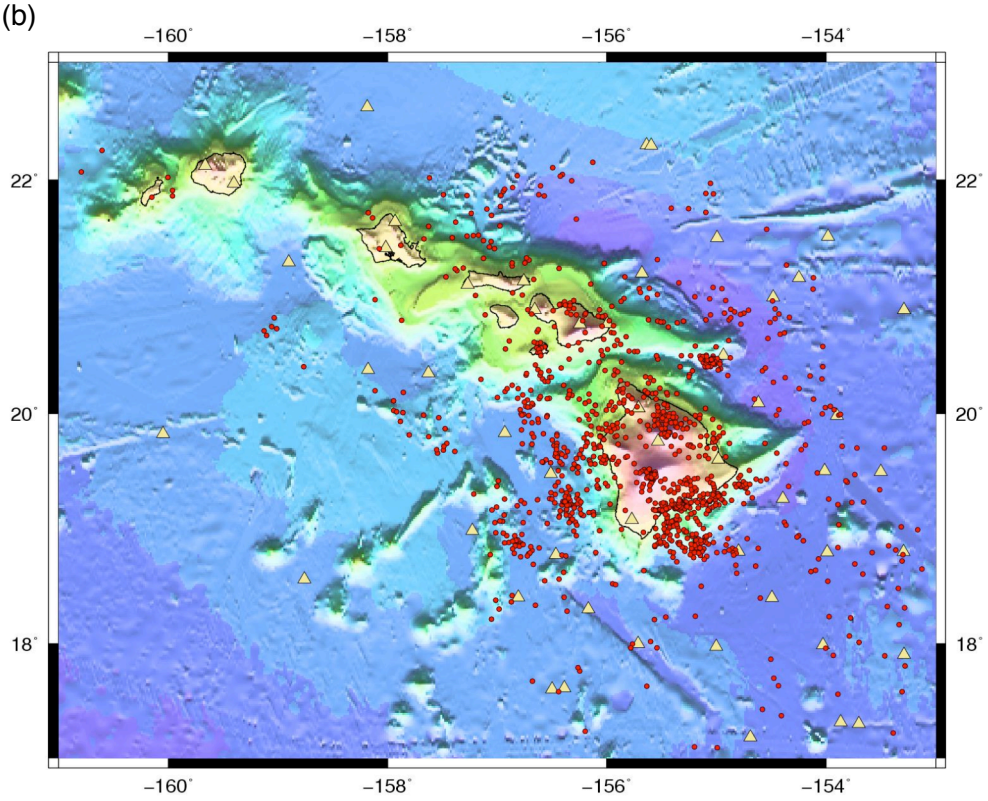

Figure 8. Epicenters of 1,147 local earthquakes detected only by PLUME. Epicentral locations are shown as red circles. Yellow triangles represent PLUME stations. Global Seismic Network stations (POHA, KIP and MAUI) are also shown. (a) Regional map. (b) Close-up view of seismicity and distribution of microearthquakes detected and located during the PLUME deployments.

4.1.1. Seismicity around the Island of Hawaii

The epicenters of 986 new events are distributed across the Big Island of Hawaii (Figure 9a). Many new earthquakes (~756) recorded in this region are located offshore of the Big Island, indicating that their locations and magnitudes may fall below the detection limit of the land-based HVO network. As expected, the HVO stations successfully documented most of the earthquake activity on land, where the PLUME analyses only revealed an additional ~230 events. It is important to note that even though the HVO effectively locates many thousands of earthquakes on the island of Hawaii and its adjacent offshore regions, a small percentage of low magnitude events may be missed, which is why PLUME detects some additional events within the HVO network. HVO locates many small (M_L < 2) events, especially if they occurred in the densely instrumented Kilauea area. However, the set of located earthquakes is nearly complete above magnitude ~2.0 [*Nakata and Okubo*, 2008].

Earthquakes in the Hawaii region (Figure 9a) are spatially diffuse around the Big Island, and although scattered seismicity occurs in the east offshore region of Hawaii, the western offshore region exhibits more focused seismic activity. For example, there is a distinct cluster of earthquakes offshore west Hawaii (~19.2°N, 156.5°W). This region was the site of a M_W 5.4 reverse faulting earthquake at 27 km depth that occurred in 1991 [*Wolfe et al.*, 2003] (see Figure 9a) and still remains seismically active.

PLUME OBSs recorded the 2005 Loihi earthquake swarm as well. Most of the offshore earthquakes situated southeast of Hawaii (18.8°N, 155.1°W) correspond to this episode. Similarly, PLUME instruments detected hundreds of aftershocks derived from

moderate to large earthquakes that occurred during the deployments. To the northeast of the island, there is a well-defined cluster of microearthquakes that followed the 2005 M_W 5.3 oblique strike slip earthquake at 12 km depth (see Figure 9a). In addition, in 2006, hundreds of aftershocks were detected after the damaging M_W 6.7 Kiholo Bay earthquake. This seismicity concentrates along the northwest coast of Hawaii. It is important to note that Figure 9a does not display many Kiholo Bay aftershocks due to the fact that the HVO network already located most of these events (see Figure 7b). Apart from the hundreds of aftershocks recorded after large earthquakes and the 2005 Loihi swarm, no other temporal patterns were noticed.

A projection of the subset of newly located hypocenters onto a North-South vertical cross section from 16.8°N to 20.7°N (Figure 8b) shows that focal depths are in the range of 1 to 75 km, with only a few events displaying greater depths. Focal depths have a pronounced bimodal distribution. Events fall into two categories: shallow events at 0-20 km below sea level and deeper events in the mantle ranging from ~25 to 60 km (see Figure 9b). Offshore seismicity far south of Hawaii (~17°N - 18.5°N) locates at shallow depths from 5 to 25 km. The depth section in Figure 9b exhibits a previously described characteristic of Hawaiian earthquakes: other earthquakes studies in the region [e.g. *Klein and Koyanagi*, 1989; *Wolfe et al.*, 2004] have shown similar depth distribution using events recorded by the HVO network during longer periods of time.

Figure 10 displays the magnitudes of the earthquakes previously discussed. In this region approximately 540 events occurred at shallow depths (< 20 km) and ~440 are located in the mantle (> 20 km). The mean magnitude for the shallow earthquakes in the

region is 1.5 and it is 1.6 for the deeper events. The largest earthquakes recorded in the area occurred offshore of the Big Island and at mantle depths.

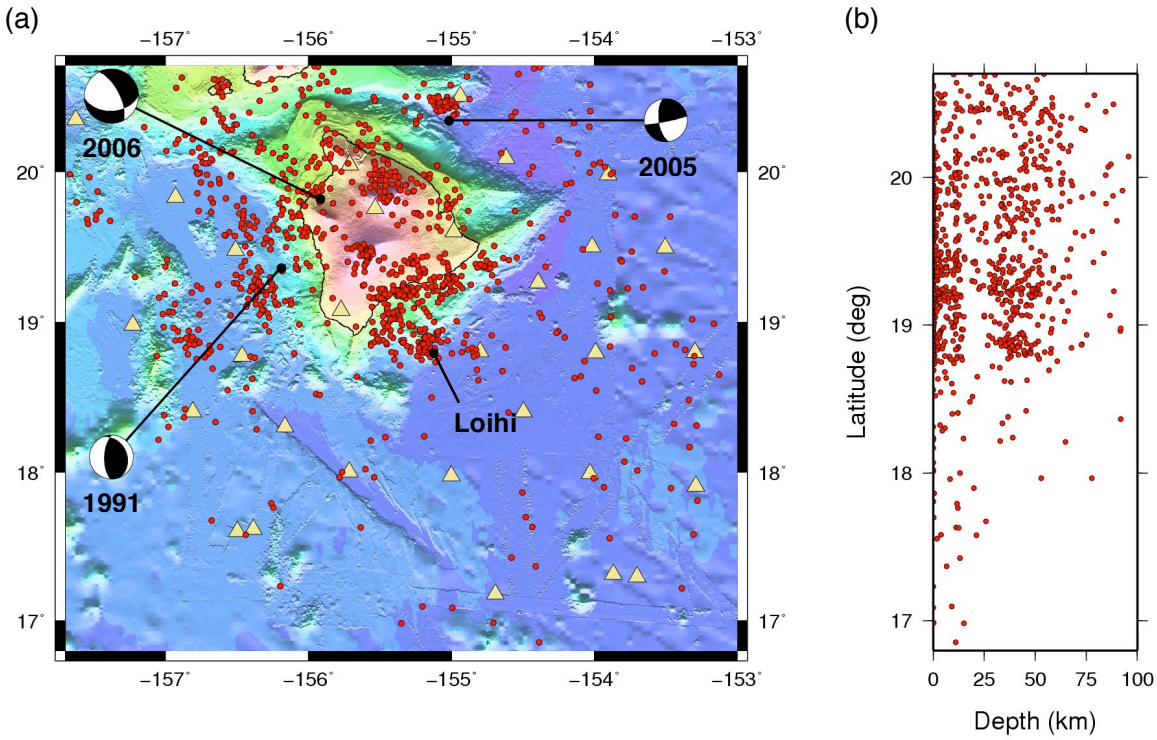

Figure 9. The epicenters and focal depths of microearthquakes located around the island of Hawaii from PLUME data. (a) Circles show the earthquake locations and triangles indicate seismometers. Focal mechanisms from *Wolfe et al.* [2003] and the Global Centroid Moment Tensor catalog illustrate the source mechanisms of three earthquakes and their years of occurrence: a oblique strike-slip MW 5.3 event in 2005, a reverse faulting MW 5.4 in 1991 and also the 2006 normal faulting MW 6.7 Kiholo Bay earthquake. The 2005 and the 2006 earthquakes occurred during the deployments and their epicentral locations are indicated by a black circle. (b) Cross-section of focal depths versus latitude (from 16.8°N to 20.7°N) for all earthquakes in the mapped region. The depths of microearthquakes range from 1 to 75 km, with the majority being divided into two sections: a shallow region from 0 to 15 km, and deeper area from 30 to 60 km.

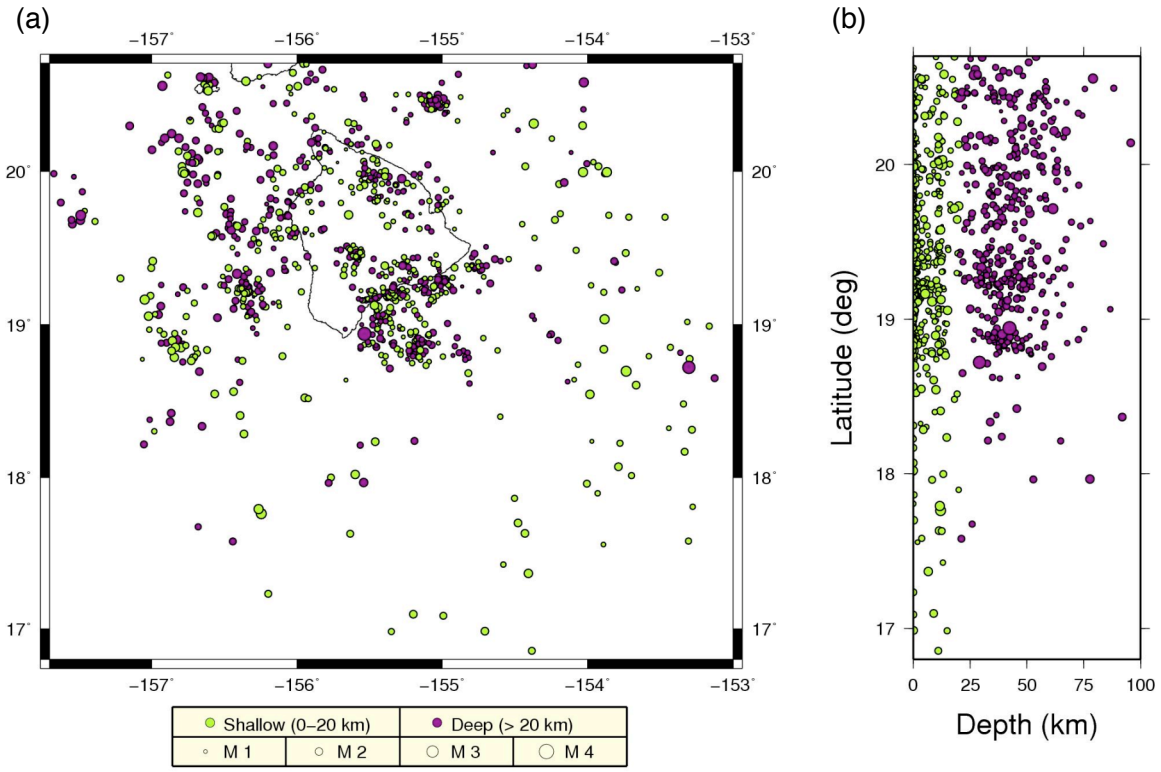

Figure 10. Estimated locations, depth distribution, and magnitudes of earthquakes located onshore and offshore Hawaii. Only those events detected solely on PLUME deployments are shown. Epicentral locations and earthquake magnitudes are represented as circles (with diameter proportional to magnitude). Focal depth is color-coded: shallow earthquakes (0-20 km) are shown in green and deeper earthquakes (>20 km) are shown in purple. (a) Map view. (b) Cross-section of depth versus latitude (from 16.8°N to 20.7°N) for all earthquakes in Figure 10a.

4.1.2. Seismicity along the islands of Maui, Molokai, Lanai and Kahoolawe

Approximately 250 earthquakes were located within this region and the epicentral locations are shown in Figure 11a. The total number of earthquakes recorded over a year in the area is ~200 during PLUME1 and ~50 during PLUME2. The average earthquake depth in the 1st deployment is 32.8 km and in the 2nd deployment is 27.6 km.

The patterns with depth are shown in a cross section in Figure 11b and a more detailed map also showing earthquakes magnitudes is displayed in Figure 12. Approximately 100 earthquakes occurred at shallow depths (0-20 km) and ~150 occurred deeper in the mantle (> 20 km). The average magnitudes are 1.8 and 1.7 for the shallow and the deep regions, respectively. The mean magnitude for events recorded during PLUME1 is 1.7 (minimum recorded magnitude: 0.7, maximum recorded magnitude: 3.3) and 2.0 (minimum recorded magnitude: 1.5, maximum recorded magnitude: 3.0) for PLUME2.

The epicentral locations of earthquakes in the region demonstrate that PLUME detected significant additional microseismicity around the islands of Maui and Molokai (Figure 11a). The spatial distribution of earthquakes reveals novel patterns. Seismicity clusters occur north of Molokai and at central Maui. A small cluster of earthquakes is evident beneath the small island of Kahoolawe. Offshore seismicity is mostly found east of Maui and north of Molokai. Beneath Maui, many earthquakes take place at mantle depths (Figure 12). These mantle microearthquakes may reflect hazardous faults similar to the one that ruptured in the 39-km-deep Kiholo Bay earthquake; although it is important to mention that the Kiholo Bay fault did not display much noticeable microseismicity prior to that earthquake [*Yamada et al.*, submitted].

The Maui region has experienced large earthquakes in the past: the 1871 and 1938 large earthquakes were suggested to be located near the island of Lanai and offshore north of Maui, respectively [*Wyss and Koyanagi*, 1992]. The events recorded by PLUME that have been located just north-eastward of Maui are deep (> 20 km) (Figure 12) and may be related to the fault zone that caused the Maui earthquake of 1938.

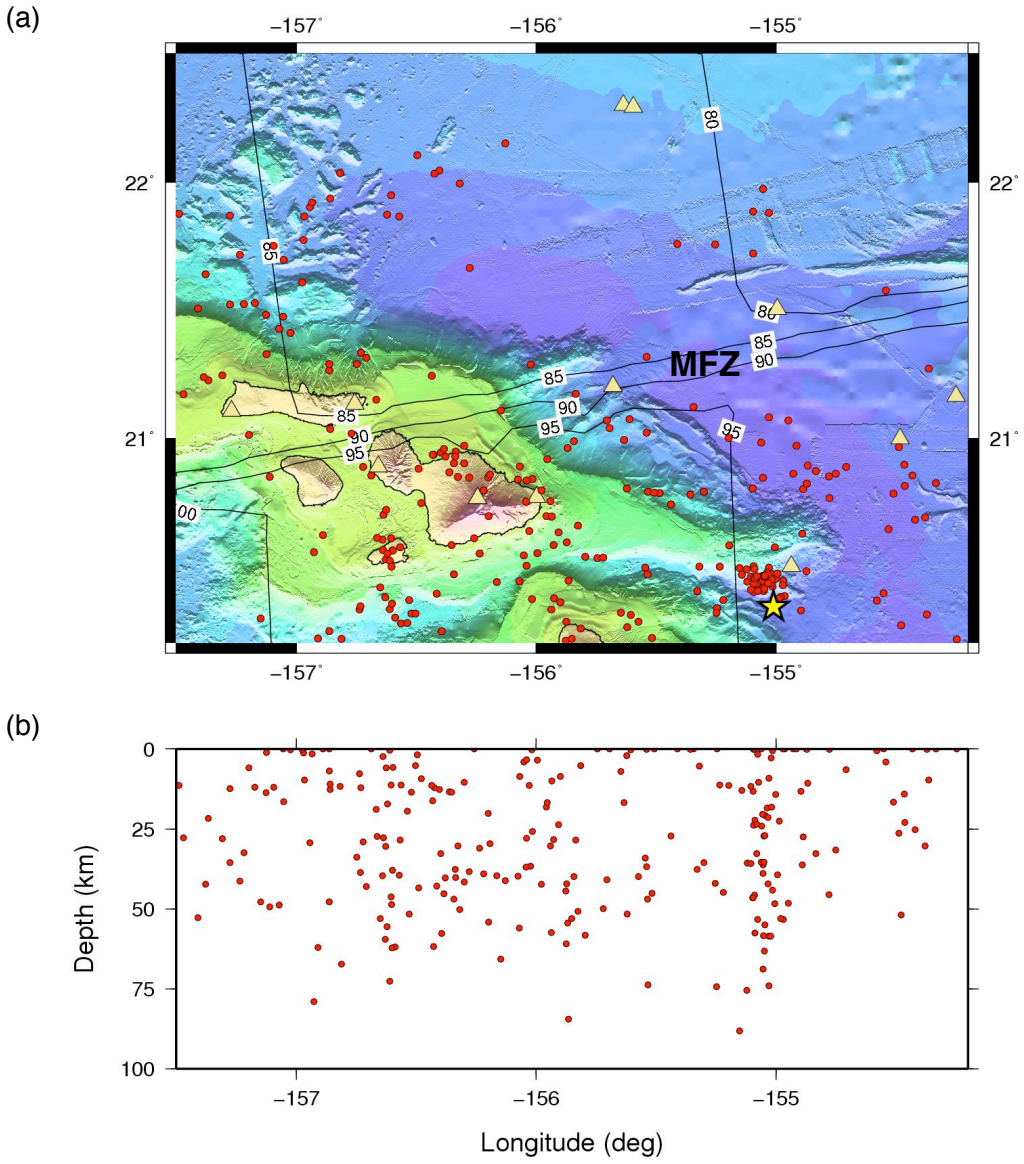

Figure 11. Epicenters and focal depths of microseismicity around the islands of Maui, Molokai, Lanai, and Kahoolawe. (a) Locations of small earthquakes (red circles) and seismic stations (yellow triangles) near Maui and neighboring islands. Yellow star indicates the location of a M_W 5.3 earthquake in 2005. Black solid lines show age contours from *Müller et al.* (1997). Seafloor ages are indicated in Ma. Offset in ocean floor age shows the location of the Molokai Fracture Zone (MFZ). (b) Cross-section of depths versus longitude (from 157.6°W to 154.2°W) for all earthquakes in the mapped region.

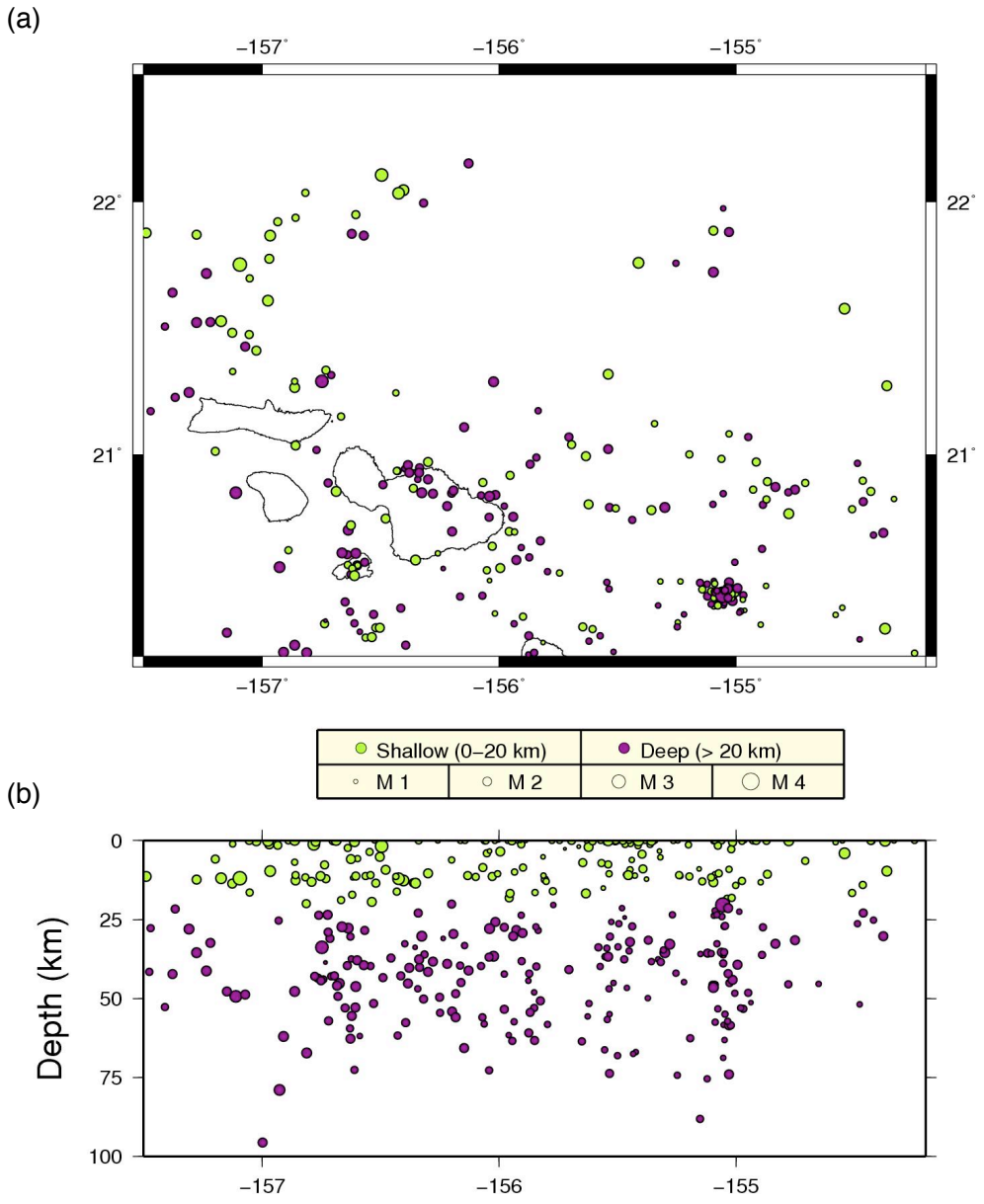

Figure 12. Estimated locations, depth distribution, and magnitudes of earthquakes located in the Maui-Molokai-Lanai region. See Figure 10 for further information. (a) Map view. (b) Cross-section of focal depths and magnitudes versus longitude (from 157.6°W to 154.2°W) for all earthquakes in Figure 12a.

PLUME data yield no evidence of ongoing seismicity on the Molokai Fracture Zone (Figure 11a). A few earthquakes do occur in the area but current seismic activity does not cluster along the fraction zone, although identification of patterns may be limited by the short duration of the PLUME deployments.

4.1.3. Seismicity along the islands of Oahu, Kauai and Niihau

The PLUME analyses located 48 small earthquakes near Oahu, Kauai and Niihau (Figure 13). The 1st PLUME deployment located 28 events in the area with a mean focal depth of 25.6 km and an average magnitude of 2.2 (minimum recorded magnitude: 1.5, maximum recorded magnitude: 3.3). The 2nd PLUME deployment located 20 earthquakes with a depth average of 34.1 km and a mean magnitude of 2.1 (minimum recorded magnitude: 1.5, maximum recorded magnitude: 3.1). A total of 19 earthquakes located at shallow depths and 29 events were located in the mantle. No temporal patterns were observed.

Figure 13 indicates that the rates of seismicity decay significantly northwest of the Big Island. The majority of the earthquakes recorded by PLUME occurred offshore to the northeast of Oahu, where 18 events were located. A small group of five microearthquakes clusters near a topographic high southwest of the island of Oahu (~28°N, 159°W). Similarly, four earthquakes cluster east of Niihau and two other earthquakes occurred farther away to the northwest of the island. No seismicity was observed near Kauai. In August 2008, a M_L= 3 earthquake was also detected and located by HVO. This earthquake generated about 50 reports of felt shaking submitted to the USGS community

internet intensity map project and was located off the Waianae coast on west side of Oahu.

The distribution of earthquake magnitudes in the region is shown in Figure 13b. Most of the seismicity appears to locate at mantle depths; however, few clusters of shallow earthquakes are also observed. Seismicity near the island of Oahu tends to be deeper and magnitudes range from 2 to 3.3.

No substantial microseismicity located near the hypothesized Diamond Head Fault. A detailed view of the seismicity in the area along with the approximate location and orientation of the Diamond Fault are shown in Figure 14. The position of the fault is as suggested by *Estill* [1979] and *Cox* [1986a]. Most of the microearthquakes in the region occur north of the putative fault and only one earthquake is observed to be on the hypothesized fault location. There is a tendency, though, for earthquakes in the region to occur in a NE-SW trend, parallel to the suggested strike of the fault. Figure 14b suggests that the seismicity near the speculated fault tends to be deep rather than shallow. Although only a few microearthquakes were recorded in the area, one caveat is that our short recording duration may be insufficient to fully characterize long-term behavior.

(a)

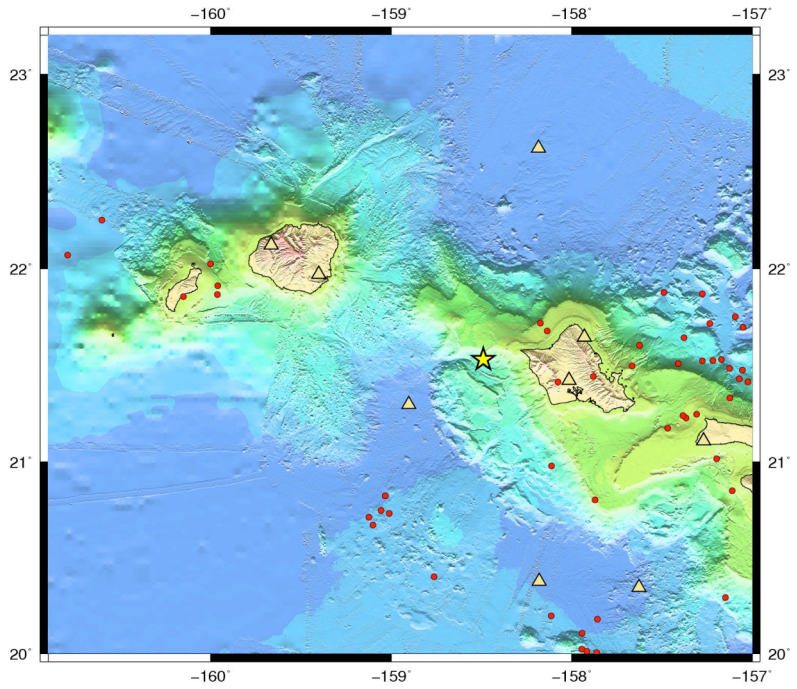
−160°
−159°
−158°
−157°
23°
22°
21°
20°

(b)

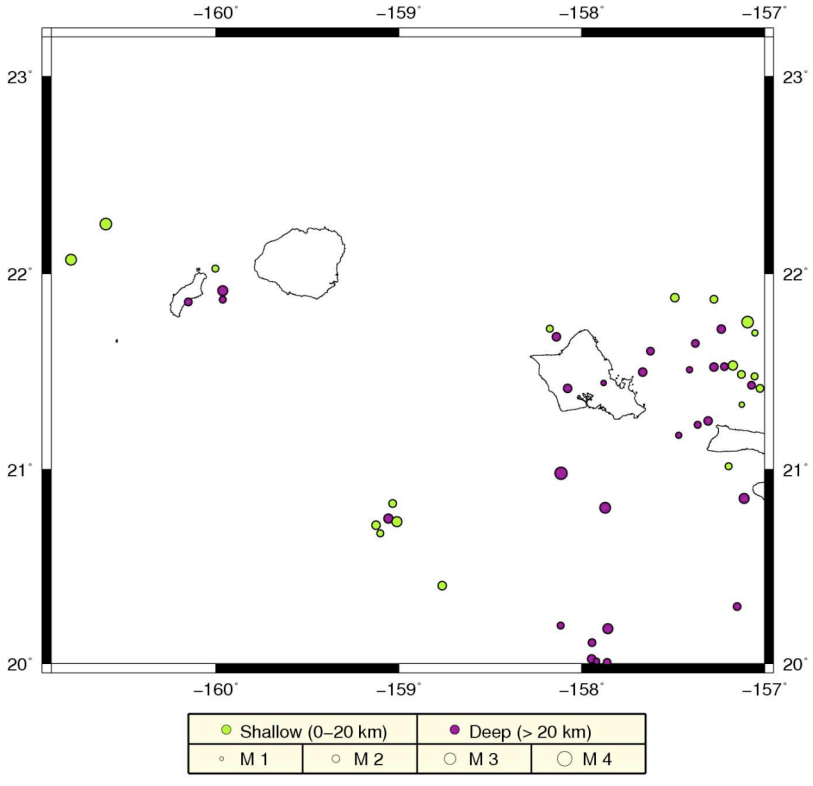
−160°
−159°
−158°
−157°
23°
22°
21°
20°
Shallow (0–20 km)
Deep (> 20 km)
M 1
M 2
M 3
M 4

Figure 13. Epicenters, depth distribution, and magnitudes of 49 small earthquakes recorded on PLUME deployments located around the islands of Oahu, Kauai, and Niihau. (a) Epicentral locations are shown in red circles. Seismic stations are shown as yellow triangles. The yellow star represents the epicentral location of the 2008 ML 3 Waianae earthquake. The Pacific Tsunami Warning Center stations registered this event and the Hawaiian Volcano Observatory scientists located it. (b) Estimated locations, depth distribution, and magnitudes of earthquakes. See Figure 10 for further information.

(a)

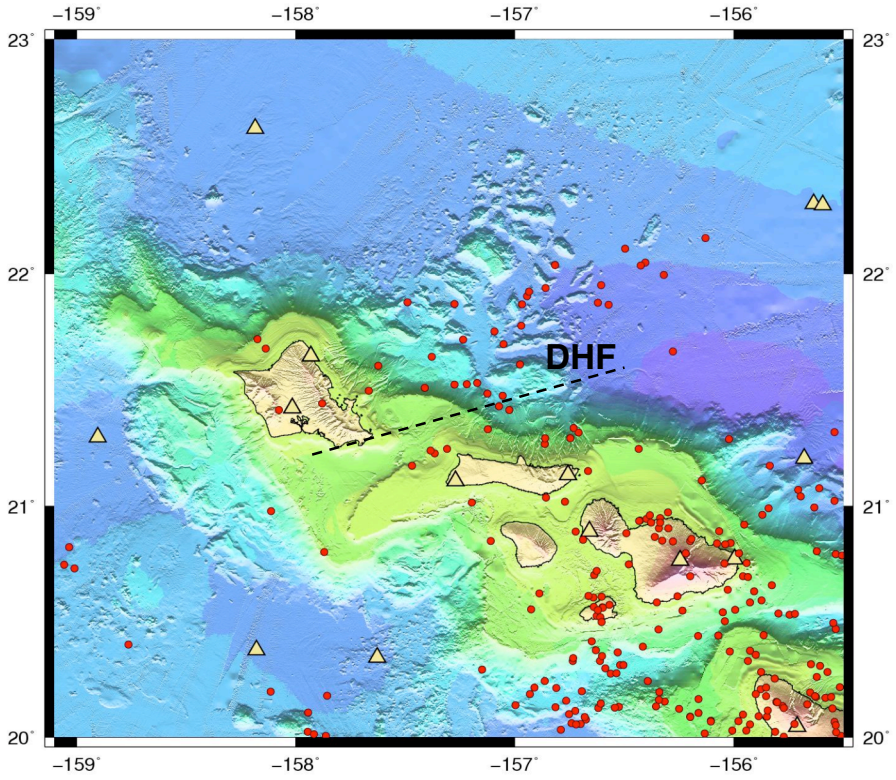
−159°
−158°
−157°
−156°
23°
22°
21°
20°
DHF

(b)

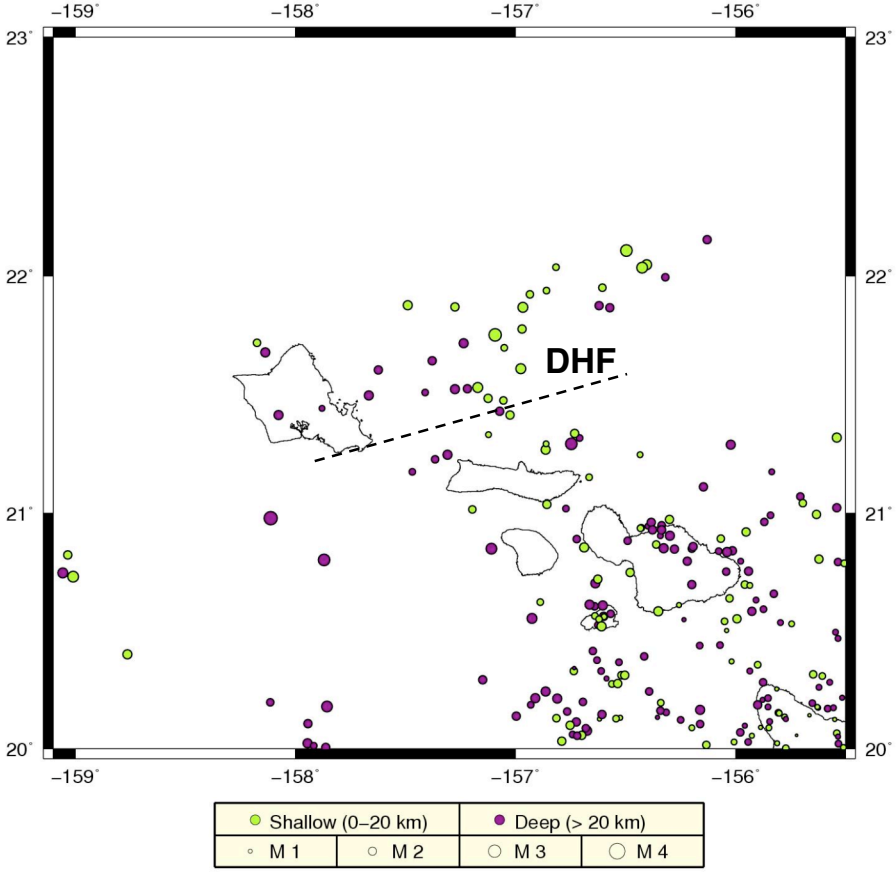
−159°
−158°
−157°
−156°
23°
22°
21°
20°
DHF
Shallow (0–20 km)
Deep (> 20 km)
M 1
M 2
M 3
M 4

Figure 14. Microearthquakes from PLUME data located around the hypothesized Diamond Head Fault. (a) Epicenters are shown as red circles, yellow triangles represent PLUME seismic stations and dashed black line indicates the approximate position and orientation of the Diamond Head Fault (DHZ) suggested by *Estill* [1979] and *Cox* [1986a]. (b) Estimated locations, depth distribution, and magnitudes of earthquakes. See Figure 10 for further information.

4.1.4. High Precision Relocations

The close spatial clustering of the microearthquakes and the repetitive waveforms at individual instruments suggests that high precision relocation techniques may improve hypocentral estimates for some events. Such techniques have been applied to subaerial microearthquakes data sets [e.g. *Got et al.*, 1994; *Sohn et al.*, 1999; *Wolfe et al.*, 2004] and have the ability to image buried faults and fractures. A double difference relocation and waveform cross correlation were applied to characterize the degree of waveform similarity and to provide differential times between pairs of seismograms for correlated events. Such approaches were unsuccessful with this dataset. The high-passed waveforms of microearthquakes on OBSs often exhibited a high degree of correlation for earthquakes that were clearly dissimilar and unrelated, thus leading to many false correlations that prohibited success with double difference relocations.

4.2. Microearthquakes: Focal Depths

Given the large station spacing of our network and large picking errors (0.5-0.6 s), focal depths are not well constrained unless an OBS is within approximately one focal depth of the epicenter. For example, in Figure 11, the aftershocks of the shallow 2005 earthquake offshore northeast Hawaii are spread over an unrealistically wide depth interval, likely due to the fact that the OBS deployed closest to this fault zone was not operational during the time period of these events.

Although there likely are some regions and time periods where depths are not well constrained, the analyses do appear to be successful in capturing the general depth

patterns. Figure 15 shows histograms of the depth distribution of earthquakes from HVO locations and the earthquakes located by PLUME.

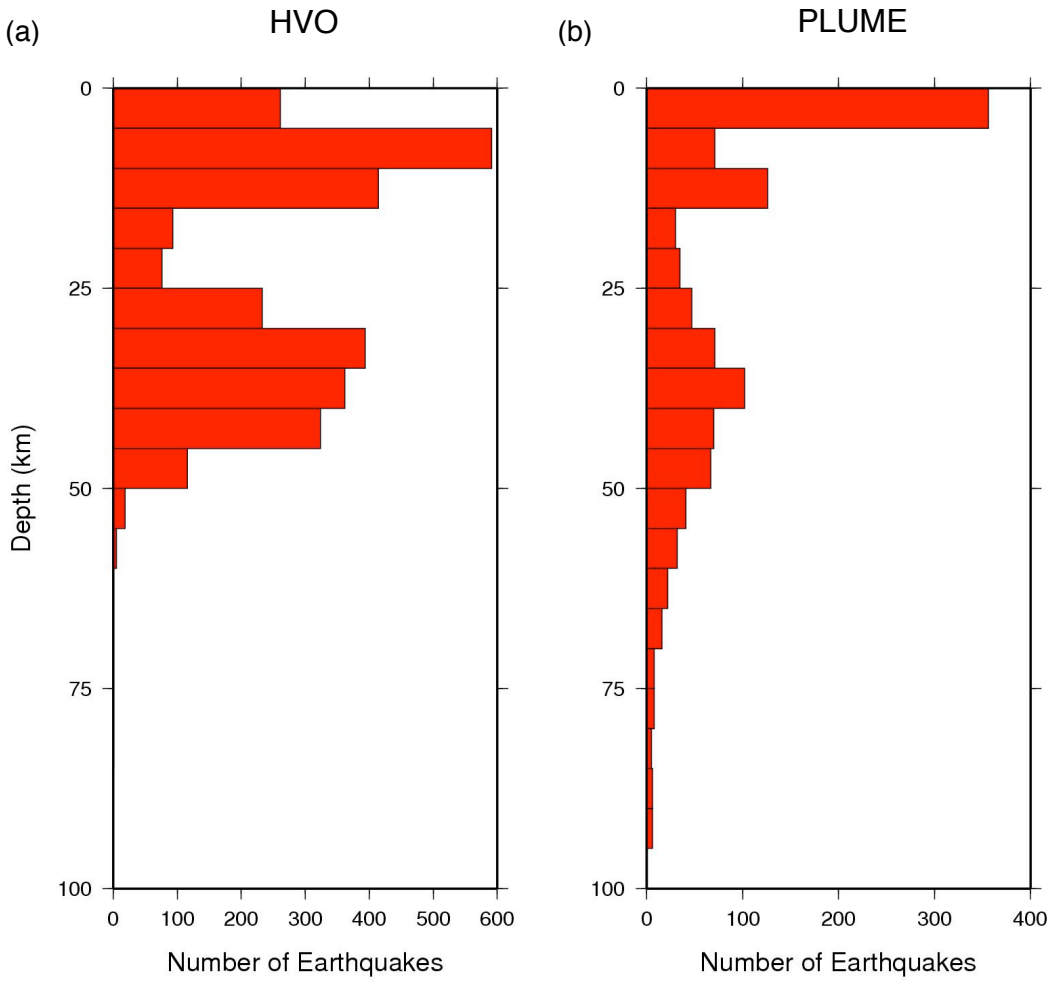

Figure 15. Histograms of earthquake depths. (a) Depths of earthquakes in the HVO catalog and detected by PLUME (see Figure 8a). (b) Depths of new microearthquakes located on the PLUME deployments (see Figure 8b). Both plots exhibit a bimodal distribution of seismicity, with two different peaks: one at crustal depths (0-15 km) and another at deeper mantle depths (35-40 km). Differences between HVO and PLUME depths patterns likely reflect differences in depth errors, and the possible influence of elevation or station corrections.

From HVO locations, it has long been recognized that the depth distribution of seismicity is bimodal, with one peak at crustal depths (10-15 km) and another peak at deeper in the mantle (25-50 km) [cf. *Klein and Koyanagi*, 1989; *Wolfe et al.*, 2004]. PLUME-derived hypocenters are sufficiently accurate to capture this bimodal pattern. However, the larger spread of depths from PLUME locations (some earthquakes located as deep as 100 km) may be a consequence of large station spacing and the large picking uncertainty.

The peak of seismicity at shallow depths (< 15 km) shown in Figure 15 reflects crustal faulting from tectonic fault zones, such as at the decollements along Mauna Loa's south flank [e.g., *Swanson et al.*, 1976; *Denlinger and Okubo*, 1995; *Nettles and Ekström*, 2004] and west flank [*Gillard et al.*, 1992; *Beiser et al.*, 1994; *Wolfe et al.*, 2004] as well as from volcanic earthquakes at Kilauea. The second peak at depths > 25 km represents mantle earthquakes likely driven by the stresses from the volcano loading and flexure of the lithosphere. In addition, *Pritchard et al.* [2007] argue that deeper earthquakes may be facilitated by high pore pressures from the exsolution of magmatic volatiles at these depths, promoting faulting at an active mantle fault zone at 30 km beneath Kilauea.

It is still not clear why seismicity declines between 15-25 km depth. It has been suggested that the low seismicity rates between 15-25 km reflects low stresses around the neutral plane of bending, dividing compressional flexural bending stresses in the upper plate from extensional bending in the lower plate. However, most flexural models for Hawaii place the neutral plane at greater depths (~25-30 km) [*Pritchard et al.*, 2007; *McGovern,* 2007], and thus contrary to this explanation. Moreover, the M_W 6.0 Mahukona aftershock of the Kiholo Bay earthquake was located at 19 km depth and its

reverse faulting mechanism indicates that it was above the neutral plane [*McGovern*, 2007], implying that the processes responsible for the decay of seismicity at depths of 15-25 km are not well understood.

The maximum depth of earthquakes in Hawaii reflects the rheology of the lithosphere and the transition in fault slip behavior from velocity-weakening at shallow depths (friction decreases with increasing sliding velocity; unstable sliding) to velocity-strengthening at deeper depths (friction increases with increasing sliding velocity; stable sliding) [*Cowie et al.*, 1993]. It is also well known that the thickness of the oceanic lithosphere and the depth of the brittle-ductile transition increase with age, due to conductive cooling [e.g. *Watts*, 2001; *Bergman and Solomon*, 1984]. By virtue of their presence, the mantle earthquakes, which are observed to ~50 km depth, help define the depth extent of the relatively old, 70-80 Myr, lithosphere beneath Hawaii.

4.3. Source Mechanisms

P-wave first motions generated by an earthquake and recorded by a number of seismographs can be used to determine a focal mechanism. Obtaining first motion focal mechanisms usually requires a dense and well-distributed network of stations around the study area, and sufficient signal-to-noise ratios to produce a robust, reasonable solution.

Source mechanisms of local microseismicity around Hawaii were particularly difficult to obtain in this study. Although reasonable local focal mechanisms were estimated for the largest events (mechanisms were already available in the Global Centroid Moment Tensor Catalog) the uneven distribution of seismographs and the total numbers of stations available to record the moderate-to-small earthquakes in such a large

area did not permit robust focal mechanism determinations for smaller events. In addition, earthquakes with smaller magnitudes tended to be recorded by fewer seismographs; this only increased the uncertainties in possible focal mechanisms. The high microseismic noise level at 1-5 Hz also makes it difficult to accurately determine the polarity of the first arrivals.

4.4. Frequency-Magnitude Distribution and *b* Values

The distribution of earthquakes sizes in a region can be described by a relationship identified by *Gutenberg and Richter* [1944]:

$$\text{Log N} = a - b\text{M}$$

where N is the cumulative number of earthquakes with magnitude larger than or equal to M, and a, b are constants that describe the activity of a seismogenic region and the relative distribution of earthquakes sizes, respectively. When plotting the log-cumulative number of earthquakes versus their magnitudes (frequency-magnitude distribution), b represents the slope of the best-fitting line for a certain magnitude range [*Aki*, 1965].

The logarithm of the number of earthquakes versus magnitude for the Hawaii and Maui-Oahu regions are plotted in Figures 16 and 17, respectively. All earthquakes detected by PLUME (including those in the HVO catalog) in the Hawaii region were used to calculate the frequency-magnitude distributions for the 1st and 2nd PLUME deployments. Figure 17 shows the earthquakes utilized for calculations in the area encompassing the islands of Maui and Oahu (latitude: 20.5˚-23.5˚N; longitude: 154˚-158.5˚W). The distributions were fitted by using a least-square fitting line to obtain *b*-values for both zones.

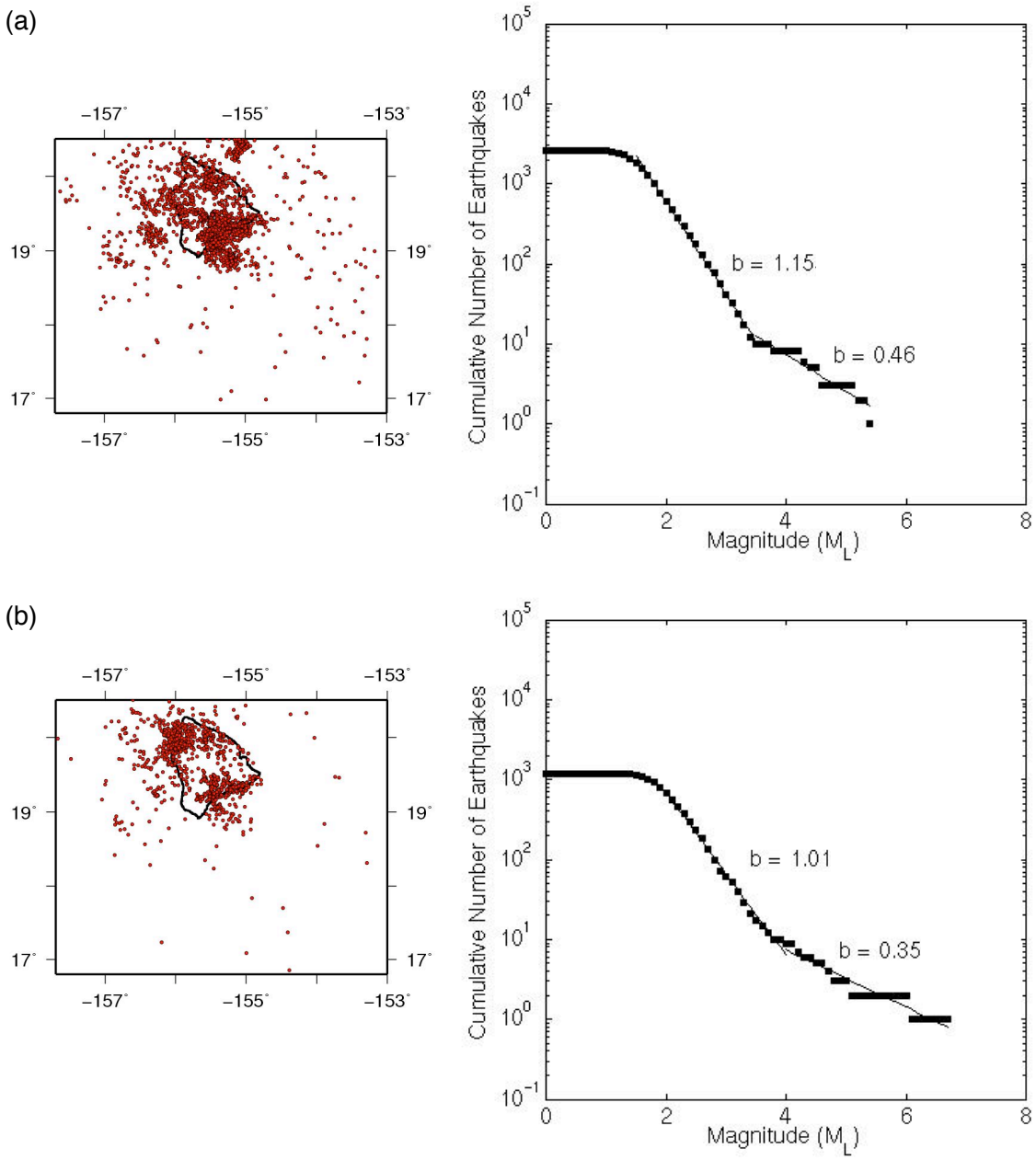

Figure 16. Frequency-magnitude distribution for earthquakes around the island of Hawaii. (a) Top row: results for the 1st PLUME deployment. (b) Bottom row: results from the 2nd PLUME deployment. First column shows the area and epicenters of earthquakes used. Second column shows cumulative counts (*N*) of earthquakes larger than *M*. Solid line are the least squares best fit of the Gutenberg-Richter relation. *b*-values from the least squares fit are also indicated.

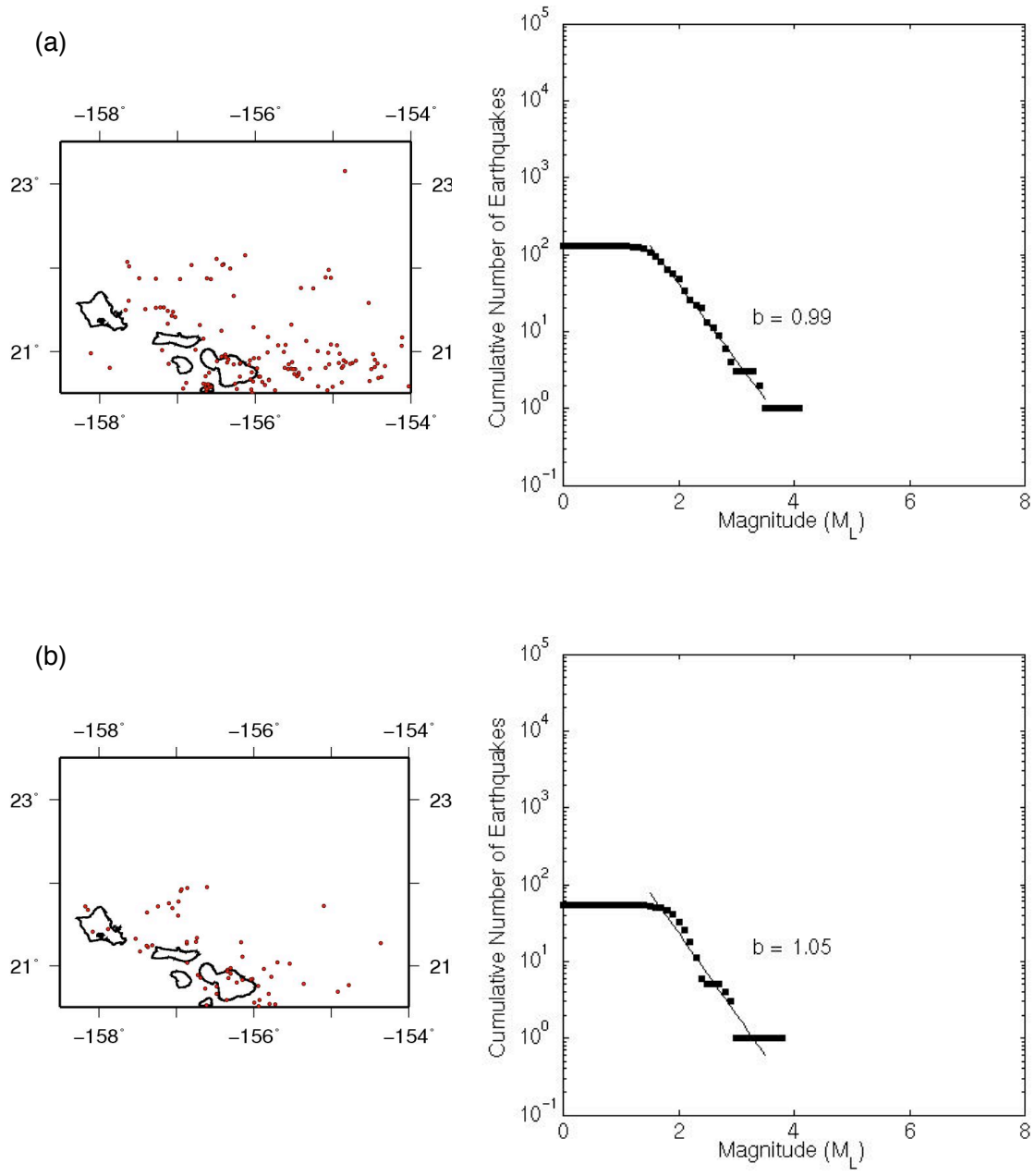

Figure 17. Frequency-magnitude distribution for earthquakes around the islands of Maui and Oahu. (a) Top row: results for the 1st PLUME deployment. (b) Bottom row: results from the 2nd PLUME deployment. See Figure 16 for further information.

The plot of the frequency of occurrence of events versus magnitude for the area of Hawaii during the 1st PLUME deployment shows a gradual curve from magnitude 1 to 3.5 (Figure 16a), whereas for the 2nd PLUME deployment (Figure 16b) the curve extends to magnitude 4.0. In both cases, the logarithm of the frequency distribution versus magnitude is approximately linear, except when the gradual detection limit is approached at lower magnitudes. The horizontal slope below $M_L \approx 1.5$ is attributed to the detection threshold. Using only events with $M_L \geq 1.5$ yields estimated *b* values of 1.15 (1st deployment, Figure 16a) and 1.01(2nd deployment Figure 16b). In the Hawaii area, a break in slope between two linear sections occurs near magnitudes ~ 3.5 and 4.0. The least squares fitted lines for magnitudes 4.0 and higher that exhibit *b* values of 0.46 and 0.35, for PLUME1 and PLUME2 respectively. For magnitudes ≥ 4.0, earthquakes tend to plot above the distribution line extrapolated from smaller magnitudes, producing the obvious change in slope of the distributions. This break in slope has been observed before for earthquakes in the region. *Klein et al.* [2001] found a similar bilinear behavior when using a much longer duration Hawaiian earthquake catalog to estimate the probabilistic hazard of the island of Hawaii. Their work shows equivalent *b* values of approximately 1 for the first slope and 0.57 for the second. Ultimately, these results suggest that the moderate to large ($M_L > 4.0$) earthquakes in the Hawaii region appear to occur more frequently than predicted by extrapolation of the Gutenberg-Richter relationship for small earthquakes. It is important to note that larger earthquakes have longer recurrence intervals and PLUME deployments each extended only one year.

For the islands of Maui and Oahu, the Gutenberg-Richter relationship indicates that the earthquake catalog from the 1st PLUME deployment is complete for $M_L \geq 1.5$,

whereas the catalog from the 2nd PLUME deployment is complete above M_L =2.0. Because the PLUME deployments are each only of 1 year duration and since large earthquakes are less frequent in the more extensive region covered by PLUME than the HVO array, only a few $M_L \geq 3$ earthquakes were recorded during the deployments. However, small earthquakes in the region produced *b* values of 0.99 (1st deployment, Figure 17a) and 1.05 (2nd deployment, Figure 17b) and no bilinear distribution is obvious.

In general, the data are well described by a Gutenberg-Richter model. Although these plots are useful only in a gross sense, the *b* value (slope) does not vary regionally for small earthquakes. Overall, seismicity recorded on PLUME deployments yield *b* values around 1.0, which are closer to typical tectonic values in Hawaii [e.g. *Klein et al.*, 2001] than the high *b* values (>1.4) that are sometimes found in volcanic regions [e.g. *Wiemer and McNutt*, 1997; *Wyss et al.*, 2001].

5. DISCUSSION

The data obtained on PLUME from 2005 through 2007 indicate some level of local seismicity (M_L 1-3.3) at onshore and offshore areas along the island chain. The majority of the microearthquakes observed on PLUME are located near the Island of Hawaii but there is some seismicity that extends northward of Hawaii, through the Maui and Molokai region to the island of Niihau. Moreover, as previously recognized by *Klein et al.* [2001], there appears to be a correlation between the number of recorded events and the distance from the Big Island (Figure 8), revealing that seismic activity lessens northwest of Hawaii. However, seismicity is not absent in these regions. Thus, the importance of having an adequate seismic network around the Hawaiian Islands is emphasized by this present study. Such a finding is not only important for earthquake monitoring, but applies to volcano monitoring as well, since Haleakala volcano on Maui is an active volcano that produced southwest rift zone eruptions at least six times in the last 1,000 years [*Bergmanis et al*., 2000].

Microearthquake locations obtained with PLUME data provide evidence of clusters of seismicity that are interpreted as active faults in the crust and upper mantle. From the island of Maui to Niihau, many onshore and offshore earthquakes appear to occur at depths greater than 20 km, reflecting active mantle fault zones. However, it should be recognized that some seismogenic fault zones may not exhibit current microseismicity: for example, *Yamada et al.* [submitted] observe that microseismicity failed to delineate the Kiholo Bay fault zone prior to the M_w 6.7 earthquake.

Mantle earthquakes in this region may not be unusual; it has been suspected that the historic 1938 Maui earthquake occurred on a mantle (~20 km) fault zone offshore northeast of Maui [*Holman*, 1982] and PLUME results provide high quality instrumental confirmation of mantle faults in the area. The 1938 event appeared to be unrelated to volcanism and it was attributed to the result from loading and bending of the Earth's crust by the mass of each Island. *Wyss and Koyanagi* [1992], based on their estimates of felt areas and patterns of intensities for the large historic Maui region earthquakes of 1871 and 1938, inferred that these two events were similar in location and magnitude. The seismicity observed in the vicinity of Maui and Molokai is interpreted in this study as related to stresses in the oceanic lithosphere associated with the loading by the islands. Similarly, the cluster of earthquakes detected by this study in the mantle near Maui's northeast coast may reflect the fault zone that was the source of the damaging 1938 Maui earthquake, as well as be a potential site of future large earthquakes.

It has long been suggested that there is a feature called the Diamond Head Fault and researchers have speculated about the possibility of an earthquake on such fault; however, both the existence of this fault and the prediction of some future events on it has been very controversial. The fault was hypothesized by *Estill* [1979] and *Furumoto et al.* [1980] on the basis of earthquakes located during a series of seismic surveys in 1976 and 1977 that were carried out using ocean-bottom seismometers. A map of epicenters of a small number of earthquakes that had been detected during the surveys show a lineation passing through Diamond Head and extending into the ocean to the northeast, such a lineation was speculated to be the Diamond Head Fault. Analogously, Estill also stated that to infer a fault from his map is probably an over-interpretation, since his locations

were very inaccurate. In the PLUME analysis, no evidence of such a fault was found. The results, instead, show earthquakes located east and northeast of Oahu (Figure 14), as well as some events north of Molokai; hence it could be possible that some of the poorly located earthquakes in Estill's work were actually situated on fault zones closer to east Oahu, such as shown by earthquakes in Figure 14. Estill's study also proposed an alternative explanation for the scattered offshore seismicity; he indicated that these may not be earthquakes on a fault but a series submarine slumps. Focal depths estimated for PLUME microseismicity near Molokai and Oahu show that many of the events that occurred at this region are deeper (> 20km), which does not favor Estill's interpretation of submarine slumping. On the basis of PLUME results it is suggested that the earthquakes found in the area correspond to the release of stresses due to the load of the Hawaiian Islands on the Pacific lithosphere. It is important to note that slumps and landslides, at all scales, occur throughout the Hawaiian Islands, especially eastern Oahu and northern Molokai [*Mark and Moore*, 1987; *Moore et al.*, 1989; *Fornari and Campbell*, 1987] thus Estill interpretation of slumping for shallower seismicity in the region may not be completely ruled out.

The 1948 "Oahu" earthquake was extensively described by *Cox* [1986a] and it is presumed that it had the second highest intensities on Oahu (first was the 1871 Lanai earthquake) of approximate magnitude VI in the Modified Mercalli (MM) intensity scale. Nevertheless there is still some concern with the intensity distribution of the earthquake, and particularly, there is debate over its exact location (see *Anonymous* [1948], *Furumoto et al.* [1973], *Furumoto et al.* [1980]). PLUME results demonstrate that seismicity is not absent around Oahu and moderate magnitude earthquakes around Oahu may be possible

in the future, although given low seismicity rates and the limited length of the historical catalogs, a quantified hazard estimate is difficult.

It is also important to note that poor historic locations of large earthquakes in the State of Hawaii such as those in 1871, 1938 and 1948 add uncertainties to seismic hazard maps. Epicentral locations of microseismicity may help improve seismic hazard calculation if seismicity can successfully delineate fault zones and clarify possible locations for future larger earthquakes. PLUME earthquake epicentral locations reveal that some offshore fault zones near Maui are seismically active. The substantial number of earthquakes at mantle depths under the island of Maui (Figures 11 and 12) is the special concern and should be taken under consideration, owing to the fact that a possible large earthquake occurring on these faults pose a threat to Maui and neighboring islands, where, in general, population and tourist industry has grown significantly over past years. Note that a large earthquake occurring on an offshore area around Maui, such where the 1938 Maui earthquake likely took place, may cause slightly less damage than an earthquake of equivalent magnitude occurring beneath the island.

From the spatial patterns of microseismicity estimated from PLUME data, the possibility of encountering seismic activity along Molokai Fracture Zone is considered. As shown in Figure 11 the epicenters of offshore seismicity in the Molokai-Maui region do not indicate current seismic activity on or near the area where the fracture zone is located. The Molokai Fracture Zone was formed when the seafloor was created, approximately 70-80 million years before the Hawaiian Islands were built [*Clague and Dalrymple*, 1987; *Atwater and Severinghaus*, 1989; *Müller et al.*, 1997]; however, it is speculated that the region produces earthquakes due to the fact that it is a zone of

weakness in which large earthquakes such as Lanai 1871 and Maui 1938 earthquakes might have occurred. The absence of current seismicity seen by PLUME suggests that the pattern of current seismic activity in the area is not to be affected by this pre-existing feature. However, the PLUME recording period may not be sufficient to define the long-term activity of the Hawaiian island region, since seismicity varies over periods of decades and even centuries.

6. CONCLUSION

The most important earthquake characteristics from this study are as follows:

1. Seismicity recorded by PLUME and HVO is spatially restricted and occurs mostly in regions near the island of Hawaii.

2. The epicentral locations of ~1200 microearthquakes detected and located during PLUME deployments suggest that numerous small earthquakes scatter along the islands. The seismic activity appears to be diffuse in some areas, however the majority of the microearthquakes clustered into three major regions: (1) Near and beneath the island of Hawaii, (2) offshore north of Maui, and (3) the northeastern regions of Molokai and Oahu.

3. The overall level of seismicity in the Maui-Molokai region appears to be higher than previously perceived, partly because the HVO network has limited detection capabilities outside the island of Hawaii. The distribution of epicenters of new microearthquakes around the islands of Maui, Molokai, Lanai and Kahoolawe suggests the existence of fault zones beneath Maui, northeastward of Maui, and north of Molokai.

4. Occasional seismicity near Oahu, Kauai and Niihau were observed. The area offshore to northeast of Oahu experienced the largest numbers of microearthquakes in this region.

5. No evidence of the Diamond Head Fault was found on PLUME analyses. Similarly, the Molokai Fracture Zone was not seismically active during the deployments. However, identification of long-term patterns may be limited by the short recording period.

6. Focal depth estimates of PLUME microearthquakes range from 1 to ~75 km. The events show a bimodal distribution with one peak at shallow depths (< 15 km) and a second peak at mantle depths (> 20 km). Earthquakes near the island of Maui, Molokai and Oahu appear are located at depths greater than 20 km, suggesting active mantle fault zones. This seismicity is interpreted as the result of stresses in the oceanic lithosphere associated with the loading by the islands.

7. A high-frequency (> 5 Hz) magnitude scale developed for PLUME earthquakes indicates that the magnitude of the newly detected events range from 0.5 to 3.5 ± 0.5 M_L units.

8. The frequency-magnitude distribution of the microearthquakes on and around the island of Hawaii appears to be bilinear. A break in slope is evident ~ M_L = 3.5 and 4.0 for datasets of PLUME1 and PLUME2, respectively. The *b* values estimated in this region for small earthquakes ($1.5 \leq M_L < 3.5\text{-}4.0$) were 1.15 (PLUME1) and 1.01 (PLUME2). Large earthquakes ($M_L \geq 3.5\text{-}4.0$) in the area exhibit *b* values of 0.46 (PLUME1) and 0.35 (PLUME2). The Maui-Oahu region reveals *b* values of 0.99 (PLUME1) and 1.05 (PLUME2) and no bilinear distribution.

LITERATURE CITED

Aki, K., Maximum likelihood estimate of b in the formula log N = a - bM and its confidence limits, *Bull. Earthquake Res. Inst. Tokyo Univ.*, 43, 237-239, 1965.

Anonymous, Seismological Notes, *Bull. Seism. Soc. Am.*, *38*, 291-299, 1948.

Atwater T. and J. Severinghaus, Tectonics maps of the northeast pacific, *The Eastern Pacific Ocean and Hawaii, The Geology Society of America*, 15-20, 1989.

Beiser, M., D. Gillard, and M. Wyss, Inversion for source parameters from sparse data sets: Test for the method and application to the 1951 (M=6.9) Kona, Hawaii, earthquake, *J. Geophys. Res.*, *99*, 19,661-19,678, 1994.

Bergman, E. A., and S. C. Solomon, Source mechanisms of earthquakes near Mid-Ocean ridges from body waveform inversion: Implications for the early evolution of oceanic lithosphere, *J. Geophys. Res.*, *89*(B13), 11,415-11,441, 1984.

Bergmanis, E. C., J. M. Sinton, F. A. Trusdell, Rejuvenated volcanism along the southwest rift zone, East Maui, Hawaii, *Bull. Volcanol., 62*, 239-255, 2000.

Caplan-Auerbach, J., and F. K. Duennebier, Seismicity and velocity structure of Loihi seamount from the 1996 earthquake swarm, *Bull. Seism. Soc. Am.*, *91*, 178-190, 2001.

Clague, D. A., and G. B. Dalrymple, Tectonics and origin of the Hawaiian-Emperor volcano chain, *The Eastern Pacific Ocean and Hawaii, The Geology Society of America*, 188-237, 1987.

Collins, J., Listening closely to 'see' into the Earth, *Oceanus Magazine*, *42*(2), 4 pp., 2004.

Collins, J. A., F. L. Vernon, J. A. Orcutt, R. A. Stephen, K. R. Peal, F. B. Wooding, F. N. Spiess, and J. A. Hildebrand, Broadband seismology in the oceans: Lessons from the Ocean Seismic Network Pilot Experiment, *Geophys. Res. Lett.*, *28*(1), 49-52, 2001.

Cowie, P. A., C. H. Scholz, M. Edwards, and A. Malinverno, Fault strain and seismic coupling on Mid-Ocean Ridges, *J. Geophys. Res.*, *98*(B10), 17,911-17,920, 1993.

Cox, D. C., The Lanai earthquake of February 1871, *University of Hawaii Environmental Center*, *SR:0034*, 50 pp., 1985.

Cox, D. C., The Oahu earthquake of June 1948, associated shocks and the hypothetical Diamond Head fault, *University of Hawaii Environmental Center*, *SR:0036*, 32 pp., 1986a

Cox, D. C., Earthquakes felt on Oahu, Hawaii and their intensities, *University of Hawaii Environmental Center*, *SR:0038*, 120 pp., 1986b.

Denlinger, R. P., and P. G. Okubo, Structure of the mobile south flank of Kilauea Volcano, Hawaii, *J. Geophys. Res.*, *100*, 24,499-24,507, 1995.

Duschenes, J., R. C. Lilwall, and T. J. G. Francis, The hypocentral resolution of microearthquakes surveys carried out at sea, *Geophys. J. R. Astron. Soc.*, *72*, 435-451, 1983.

Estill, R. E., Seismotectonics and velocity structure of the southeastern Hawaiian Ridge, Ph.D. dissertation, University of Hawaii at Manoa, Honolulu, 1979.

Fornari, D. J. and J. F. Campbell, Volcanic hazards in the Hawaiian Islands, in *Volcanism in Hawaii*, edited by R. W. Decker and T. L. Wright, *U.S. Geol. Surv. Prof. Pap. 1350*, 109-124, 1987.

Furumoto, A. S., N. N. Nielsen, and W. R. Phillips, A study of past earthquakes, isoseismic zones of intensity and recommended zones for structural design for Hawaii, *Engineering Bulletin PACE 72033, Center for Engineering Research, University of Hawaii*, 1973.

Furumoto, A. S., W. Lum, N. N. Nielsen, and J. T. Yamamoto, A Study of earthquake losses in the Honolulu area: Data and analysis, *Dept. of Defense Civil Defense Division, State of Hawaii*, 1980.

Furumoto, A. S., E. Herroro-Bevera and W. M. Adams, Earthquake risk and hazard potential of the Hawaiian Islands, *Hawaii Institute of Geophysics, University of Hawaii*, 36 pp., 1990.

Gillard, D., M. Wyss, and J. S. Nakata, A seismotectonic model for western Hawaii based on stress tensor inversion from fault plane solutions, *J. Geophys. Res.*, *97*, 6629-6641, 1992.

Got, J. L., J. Frechet, and F. Klein, Deep fault plane geometry inferred from multiplet relative relocation beneath the south flank of Kilauea, *J. Geophys. Res.*, *99*, 15,375-15,386, 1994.

Gutenberg, B. and C. F. Richter, Frequency of Earthquakes in California, *Bull. Seism. Soc. Am.*, *34*, 185-188, 1944.

Holman, C. H., Crustal deformation, and seismic risk from earthquakes in Maui, Molokai, and Lanai, M.S. Thesis, University of Hawaii at Manoa, Honolulu, 1982.

Klein, F. W., and R.Y. Koyanagi, The seismicity and tectonics of Hawaii, in *The Eastern Pacific Ocean and Hawaii,* edited by E. L. Winterer, D. M. Hussong and R. W. Decker, *Geological Society of America, N,* 238-252, 1989.

Klein, F. W., and T. L. Wright, Catalog of Hawaiian earthquakes 1823-1959, *U.S. Geol. Surv. Prof. Pap.*, *1623*, 90 pp., 2000.

Klein, F. W., A. D. Frankel, C. S. Mueller, R. L. Wesson, and P. G. Okubo, Seismic hazard in Hawaii: High rate of large earthquakes and probabilistic ground-motion maps, *Bull. Seism. Soc. Am.*, *91*(3), 479-498, 2001.

Laske, G., J. A. Collins, C. J. Wolfe, S. C. Solomon, R. S. Detrick, J. A. Orcutt, D. Bercovici and E. H. Hauri, The Hawaiian PLUME Project – Probing a Hotspot with State-of-the-Art Ocean Bottom Seismometers, *Eos Trans. AGU*, submitted.

Levenberg, K., A method for the solution of certain nonlinear problems in least squares, *Quantitative and Applied Mathematics*, *2*, 164-168, 1944.

Lipman, P. W., J. P. Lockwood, R. T. Okamura, D. W. Swanson, and K. M. Yamashita, Ground deformation associated with the 1975 magnitude-7.2 earthquake and resulting changes in activity of Kilauea Volcano, Hawaii, *U.S. Geol. Surv. Prof. Pap*. *1276*, 45 p., 1985.

Mark, R. K. and J. G. Moore, Slopes of the Hawaiian Ridge, in *Volcanism in Hawaii*, edited by R. W. Decker and T. L. Wright, *U.S. Geol. Surv. Prof. Pap. 1350*, 101-107, 1987.

Marquardt, D. W., An algorithm for least-squares estimation of nonlinear parameters, *SIAM Journal*, *11*, 431-441, 1963.

McGovern, P. J., Flexural stresses beneath Hawaii: Implications for the October 15, 2006, earthquakes and magma ascent, *Geophys. Res. Lett.*, *34*, L23305, 2007.

Moore J. G., D. A. Clague, R. T. Holcomb, P. W. Lipman, W. R. Normark, and M. E. Torresan, Prodigious submarine landslides on the Hawaiian Ridge, *J. Geophys. Res.*, *94*, 17,465-17,484, 1989.

Müller, R. D., W. R. Roest, J.-Y. Royer, L. M. Gahagan, J. G. Sclater, Digital isochrones of the world's ocean floor, *J. Geophys. Res., 102*, 3211-3214, 1997.

Mullineaux D. R., D. W. Peterson, and D. R. Crandell, Volcanic hazards in the Hawaiian Islands, in *Volcanism in Hawaii*, edited by R. W. Decker and T. L. Wright, *U.S. Geol. Surv. Prof. Pap. 1350*, 599-621, 1987.

Nakata, J. S., Hawaiian Volcano Observatory Seismic Data, January to December 2006, *U.S. Geol. Surv. Open File Rep.*, *2007-1073*, 100 pp., 2007.

Nakata, J. S., and P. G. Okubo, Hawaiian Volcano Observatory Seismic Data, January to December 2007, *U.S. Geol. Surv. Open File Rep.*, *2008-1261*, 99 pp., 2008.

Nettles, M., and G. Ekström, Long-period source characteristics of the 1975 Kalapana earthquake, *Bull. Seism. Soc. Am.*, *94* (2), 422-429, 2004.

Owen, S. R, R. Denlinger, M. Sako, P. Segall, M. Lisowski, and A. Miklius, Rapid deformation of Kilauea Volcano: Global Positioning System measurements between 1990 and 1996, *J. Geophys. Res.*, *105*, 18,983-18,998, 2000.

Pavlis, G. L., F. Vernon, D. Harvey, D. Quinlan, The generalized earthquake-location (GENLOC) package: an earthquake-location library, *Computers & Geosciences*, *30*, 1079-1091, 2004.

Pritchard, M. E., A. M. Rubin, and C. J. Wolfe, Do flexural stresses explain the mantle fault zone beneath Kilauea volcano?, *Geophys. J. Int.*, *168*, 419-430, 2007.

Shiro, B. R., S. K. Koyanagi, P. G. Okubo, and C. J. Wolfe, Towards the establishment of the Hawaii Integrated Seismic Network for tsunami, seismic, and volcanic hazard mitigation (abstract), *Eos Trans. AGU*., *2006 Fall Meeting*, T23A-0475, 2006.

Sohn, R. A, J. A. Hildebrand, and S. C. Webb, A microearthquake survey of the high-temperature vent fields on the volcanically active East Pacific Rise (9°50'N), *J. Geophys. Res.*, *104*, 25,367-25,377, 1999.

Stein, S., and M. Wysession, An introduction to Seismology, Earthquakes, and Earth Structure, *Blackwell Publishing*, 498 pp., 2003.

Swanson, D. A., W. A. Duffield, and R. S. Fiske, Displacement of the south flank of Kilauea Volcano; the result of forceful intrusion of magma into the rift zones, *U.S. Geol. Surv. Prof. Pap. 963*, 1976.

Unger J. D., and P. L. Ward, A large, deep Hawaiian earthquake: the Honomu, Hawaii event of April 26, 1973, *Bull. Seism. Soc. Am.*, *69*(6), 1771-1781, 1979.

Watts, A. B., Isostasy and Flexure of the Lithosphere, *Cambridge University Press*, 458 pp., 2001.

Watss, A. B., and U. S. ten Brink, Crustal structure, flexure, and subsidence history of the Hawaiian Islands, J. Geophys. Res., *94*, 10,473-10,500, 1989.

Webb, S. C., Broadband seismology and noise under the ocean, *Reviews of Geophysics*, *36*, 105-142, 1998.

Wiemer, S. and S. R. McNutt, Variations in the frequency magnitude distribution with depth in two volcanic areas: Mount St. Helens, Washington, and mount Spurr, Alaska, *Geophys. Res. Lett.*, *24*, 189-192, 1997.

Wilcock, W. S. D., and D. R. Toomey, Estimating hypocentral uncertainties for microearthquakes surveys conducted at sea: A comparison of generalized inverse and grid search methods, *Mar. Geophys. Res.*, *13*, 161-171, 1991.

Wolfe, C. J., P. G. Okubo and P. M. Shearer, Mantle fault zone beneath Kilauea Volcano, Hawaii, *Science*, *300*, 478-480, 2003.

Wolfe, C. J., P. G. Okubo, G. Ekstrom, M. Nettles, and P. M. Shearer, Characteristics of deep (³13km) Hawaiian earthquakes and Hawaiian earthquakes west of 155.55°W, *Geochem. Geophys. Geosyst.*, *5*, Q04006, doi:10.1029/2003GC000618, 2004.

Wright, T. L., and F. W. Klein, New catalog reexamines Hawaii's seismic history, *Eos Trans. AGU, 81*, 101-102, 2000.

Wyss, M., and R. Y. Koyanagi. Isoseismal maps, macroseimic epicenters and estimated magnitudes of historic earthquakes in the Hawaiian Islands, *U.S. Geol. Surv. Bulletin 2006*, 93 pp., 1992.

Wyss, M., F. Klein., K. Nagamine and S. Wiemer, Anomalously high b-values in the South flank of Kilauea volcano, Hawaii: evidence for the distribution of magma

below Kilauea's East rift zone. *J. Volcanology Geothermal. Res.*, *106*, 23-37, 2001.

Yamada, T., P. G. Okubo, and C. J. Wolfe, The 2006 Kiholo Bay earthquake sequence: Relationship of the main shock slip with locations and source parameters of aftershocks, *J. Geophys. Res.,* submitted.

Zucca, J. J., D. P. Hill, and R. L. Kovach, Crustal structure of Mauna Loa Volcano, Hawaii, from seismic refraction and gravity data, *Bull. Seismol. Soc. Am.*, 72,1535-1550, 1982.